Hindawi
Shock and Vibration
Volume 2024, Article ID 5363146, 25 pages
https://doi.org/10.1155/2024/5363146

Research Article

Pole Allocation Applied to Two Buildings Connected by Joint Damper

Yoshiki Ikeda[1] **and Yuki Matsumoto**[2]

[1]*Disaster Prevention Research Institute, Kyoto University, Kyoto, Japan*
[2]*Graduate School of Engineering, Kyoto University, Kyoto, Japan*

Correspondence should be addressed to Yoshiki Ikeda; ikeda.yoshiki.6r@kyoto-u.ac.jp

Received 3 November 2023; Revised 3 January 2024; Accepted 16 January 2024; Published 27 January 2024

Academic Editor: Manoj Khandelwal

Copyright © 2024 Yoshiki Ikeda and Yuki Matsumoto. This is an open access article distributed under the Creative Commons Attribution License, which permits unrestricted use, distribution, and reproduction in any medium, provided the original work is properly cited.

For two adjacent buildings connected by a joint damper, an inverse problem is formulated based on the pole allocation method in control theory. The structural system is simplified as a two-degrees-of-freedom (2-DOF) lumped-mass damped shear model. The unified governing equation, which expresses the relationship between an assigned control target and the structural parameters for an earthquake-resistant building, seismically isolated building, or passively controlled building, is extended to structural control using a joint damper. The introduced equation automatically constrains the variations in the structural parameters under the assigned modal properties. The integration of the pole allocation method and fixed-point theory directly estimates the additional damping effect on the target buildings from the optimum capacity of the joint damper, which improves the trial-and-error steps at the preliminary design stage. The past fixed-point theories do not provide the additional damping effect but the optimum damping coefficient of the joint damper. The present study directly links the additional damping with the damping of the joint damper. Numerical examples are used to verify the theoretical integration using a 20-DOF building model wherein two 10-DOF models are connected by a joint damper between the top lumped masses.

1. Introduction

The pole allocation method, which is widely used in control engineering, has already been applied to a multilumped mass stick-shaped shear model and determined that there is a mathematical equation governing the vibration of buildings [1–4]. This equation is referred to as either a unified or governing equation [3, 4]. For a base-isolated structure, interstory-isolated structure, or passively controlled structure using tuned mass dampers (TMDs) or interstory viscous dampers, the equation constrains the variations in the structural parameters and control devices by specifying the poles. These poles correspond to the natural frequencies and damping ratios of the vibration modes, and they serve as control targets. The introduced equation aids in physically understanding the control effect of seismic isolation and passive dampers and helps improve the trial-and-error TMD design [1, 2]. Pole allocation is related to the performance-based design in structural dynamics because the application starts by assigning a control target to the vibration modes. In this study, first, the unified description considering the vibration of one building is extended to two adjacent buildings connected by a joint damper. Subsequently, the introduced closed-form description is integrated with the fixed-point theory because the theory does not provide the structural damping effect; rather, it provides the optimum damping coefficient for the joint damper. This integration directly links the structural damping with the damping of the joint damper. Consequently, a simple method is proposed at the preliminary design stage to predict additional structural damping without dynamic analysis.

Passive joint damper is a structural control strategy aimed at reducing the vibration of one or two buildings by connecting them [5–31]. The authors in [5, 6] proposed the optimization of a joint damper in simple uniform shear beam models representing two adjacent buildings of

different heights. From the perspective of the optimization of lumped-mass models, a majority of the research on joint dampers is derived from the fixed-point theory applied to a two-degrees-of-freedom (2-DOF) system wherein two single-degree-of-freedom (S-DOF) undamped models are connected using a dashpot [7]. The application of a 2-DOF system with a joint damper is an extension of the fixed-point theory for an S-DOF undamped model with a TMD [8]. When the two S-DOF models are undamped, two fixed points appear in the frequency transfer functions of the structural response to excitation. These points cannot be moved by changing the damping coefficient of the dashpot. The fixed-point theory determines the damping coefficient to ensure that the transfer functions for the S-DOF models achieve the same peak value at two fixed points. This is because the heights of the transfer functions cannot be lowered below the fixed points, which are often referred to as points P and Q [7, 8]. The optimum damping coefficient at each fixed point can be obtained by solving the corresponding quadratic equation. The fixed-point theory employs the average of the two optimum damping coefficients for the dashpot. This theory proposes an optimization approach to determine damper capacity as a damping coefficient and has become a standard design method for joint dampers. Essentially, a damper is selected to minimize the frequency response in the first and second modes of the structural system. The original fixed-point theory selects the base and structural displacements as the input and outputs of the structural system, respectively, in the transfer functions [7]. This theory is derived using a similar mathematical process wherein accelerations are the input and outputs [9]. The authors in [9] confirmed through numerical examples that the damping of connected structures does not have a significant effect on optimization. This unnoticeability supports the two S-DOF undamped models in the fixed-point theory.

The early fixed-point theory in [7] was extended to a 2-DOF model wherein a spring was placed parallel to the dashpot between two S-DOF undamped models; however, this optimization was proposed for numerical analysis [10]. Subsequently, corresponding closed-form solutions were introduced for the same problem [11–13]. When a spring is inserted between the two S-DOF models, a control effect can be obtained, even when the mass ratio between the two S-DOF models is one. The spring-dashpot parallel arrangement is known as the Kelvin–Voigt model. The introduced closed-form optimizations simplify the design process of the coupling structures. The optimizations can be applied to various transfer functions, where the input is the base displacement, velocity, or acceleration and the outputs are structural displacements or accelerations. However, when the spring value increases, the optimum damping coefficient defined in the early fixed-point theory cannot be obtained, because the peak values at the two fixed points differ significantly. The authors in [11] stated that there is a fixed-point independent of the connecting spring, which can better explain the characteristics of frequency transmissibility using the closed-form expression. Thus, the corresponding system is independent of the Kelvin–Voigt model. The authors in [11] highlighted that when the product of the mass and stiffness ratios between the two S-DOF models is constant, the connecting spring is not necessary. The conspicuous case for necessity is limited to when the masses of the two models differ significantly, and the natural frequency of an S-DOF model with a smaller mass is lower than that of another S-DOF model with a larger mass. This may be a rare case, wherein two buildings with almost the same height are adjoined. A joint damper is a structural control strategy that uses the difference between the dynamic properties of two buildings. The connecting spring aligned the seismic responses of both buildings, which may have caused slight contradictions. Although the authors in [7, 9–13] focused on a 2-DOF model, they solved the significant problem of determining the optimum damper parameters. However, these fixed-point theories do not provide the structural damping effect but the optimum damping coefficient of the joint damper. The present study directly links structural damping with the damping of the joint damper by integrating pole allocation and the fixed-point theory.

Some closed-form solutions for the optimum parameters of the Kelvin–Voigt damper model have been provided using the eigenvalue problem [14–16] and by minimizing the time-averaged energy of the two buildings [17]. Parametric studies have highlighted the presence of a distinct point where two complex eigenvalues coincide, thus leading to the maximum value of one of the two damping ratios [18]. The authors in [14] improved the structural control effect by increasing the damping ratios in the first vibration modes of two adjacent structures. The improvement yielded the same maximum damping ratio in the first modes under the condition that the two natural frequencies in the first modes are equal. Essentially, when the product of the mass and stiffness ratios is constant, the additional damping ratios for the two S-DOF models become the same [11, 15, 16]. The studies in [14, 18] first clarified the fundamental dynamic properties of joint damper from the viewpoint of modal damping maximization; furthermore, it highlighted the distinct point at which the two complex eigenvalues coincide with the maximum damping ratio. Even if the product is not constant, the effect can be similar within the practical range of the dashpot capacity [16]. The optimization in the studies in [14] may be acceptable in applications owing to the same damping ratio for the two structures, whereas the condition of the first same natural frequencies may be too strong for the adjacent structures. The consideration of structural damping is a new viewpoint compared with the fixed-point theory. The studies in [15, 16, 18] follow the studies in [14].

When the fixed-point theory is applied to the 2-DOF model with the Kelvin–Voigt connection, its modal characteristics are classified into three types based on the mass and frequency ratios between the two S-DOF models [19]. This classification also provides a joint damper from a contrasting viewpoint, compared with that of fixed-point theories. A similar characteristic was expressed in a closed form for the early 2-DOF model with only a dashpot [16]. This expression indicates that the modal characteristics depend on the relationship between the mass and stiffness

ratios of the two buildings. The authors in [16] presented another perspective wherein the modal characteristics change in conjunction with the dashpot capacity. This phenomenon has been overlooked in fixed-point theories emphasizing dashpot optimization. Thus, the present study also considers the relationship between the structural damping and dashpot capacity.

Joint dampers have been proposed to suppress the vibration of a single building, for example, seismic retrofitting using outer frames [20], exoskeleton structures [21, 22], double-skin facades [23–26], and inertial mass dampers [27]. In studies involving applications, the main structures are typically connected to uncontrolled substructures using dashpots and/or springs. Thus, reducing the response of a building may be relatively easy because the dampers work on the principle of absorbing seismic energy by moving themselves, and the substructure works as a damper. However, in practical applications, a standard design is used to suppress the responses of the two buildings. This study aims to address this research gap by suppressing the seismic responses of two buildings with different natural frequencies at the same level.

A design procedure with higher generality was established to consider different control targets: the minimum response of one building, minimum response peak, balance of the dynamic behavior, and in any case for both accelerations and displacements [28]. The minimization of the total energy is strongly linked to high damping effect [28], which follows the modal damping maximization described in [14]. The authors in [15, 18, 28] indicated design maps with nondimensional structural parameters for a clear understanding of the dynamic properties of joint damper control. However, the understanding of the dynamic characteristics, particularly the control effect, in parametric and numerical analyses may not be required at the preliminary design stage [15, 18, 28–31]. This existing research requires further advancement to estimate the control effect in a closed form based on the capacity of the damper.

Application examples include one damper connecting two adjacent buildings [6] and multiple dampers connecting different floors [20, 29, 30]. This study focuses on a case of two adjacent buildings of almost the same height, with a joint damper installed near both their top floors to simultaneously reduce the vibration of the buildings. The viscous joint damper is assumed to maintain an ideal state in which no friction occurs at the joint and the damping force is directly applied to the two buildings. This study applies the pole allocation method that assumes a linear system. Although nonlinearity in structures and control devices should be considered in practical designs of structural control systems, the nonlinear behaviors are out of this study. The focus on linear performance has three following reasons: (1) this study aims to introduce a basic equation which can easily understand the relation between additional damping effect and damper's capacity at the preliminary design stage for a joint damper; (2) to decrease the repair effort after a large earthquake, structural control technologies have been expected to be able to control, as much as possible, the seismic responses during an earthquake within the elastic ranges of structural members; and (3) actually and generally, the preliminary design stage for controllers considers the linear region in which they work most effectively.

The remainder of this paper is organized as follows. Section 2 extends the unified description for the vibration of one building to two adjacent buildings connected by a joint damper, based on the pole allocation method. It integrates the unified description with the fixed-point theory to predict the additional damping effect on two adjacent buildings. Section 3 presents the fundamental characteristics of the prediction equation for the damping effect. Section 4 presents the application of the prediction equation for the damping effect in a structural system wherein two multi-degrees-of-freedom (M-DOF) stick-shaped shear models are connected by a joint damper on the top floors. Similar to this paper, the authors in [7, 9–13, 15–19, 21, 22] handle 2-DOF systems which link S-DOF systems with a joint damper. Although the authors in [14, 20] initially make M-DOF systems, they finally simplify the M-DOF systems into 2-DOF systems. The authors in [14] approximate the M-DOF system as the corresponding 2-DOF system by using the first-modal information. The authors in [23–25] utilize M-DOF systems with numerical analyses. Considering the current facts, theoretical approaches to joint damper may be limited within a 2-DOF system. Section 4 reports an extension of the formulation developed for the 2-DOF system to M-DOF systems. Finally, Section 5 concludes the study.

2. Pole Allocation Applied to Joint Damper

2.1. Equation of Motion and State Equation. When two S-DOF damped structures are passively controlled by a joint damper, as shown in Figure 1, the equation of motion can be expressed as follows:

$$\begin{bmatrix} m_A & 0 \\ 0 & m_B \end{bmatrix} \begin{Bmatrix} \ddot{x}_A \\ \ddot{x}_B \end{Bmatrix} + \begin{bmatrix} c_A + c_J & -c_J \\ -c_J & c_B + c_J \end{bmatrix} \begin{Bmatrix} \dot{x}_A \\ \dot{x}_B \end{Bmatrix} + \begin{bmatrix} k_A + k_J & -k_J \\ -k_J & k_B + k_J \end{bmatrix} \begin{Bmatrix} x_A \\ x_B \end{Bmatrix} = -\begin{bmatrix} m_A & 0 \\ 0 & m_B \end{bmatrix} \begin{Bmatrix} 1 \\ 1 \end{Bmatrix} \ddot{y}_0, \tag{1}$$

where m_A is the lumped mass of building A, m_B is the lumped mass of building B, k_A is the shear stiffness of building A, k_B is the shear stiffness of building B, k_J is the axial spring connecting buildings A and B, c_A is the damping coefficient of building A, c_B is the damping coefficient of building B, c_J is the damping coefficient of the dashpot connecting buildings A and B, x_A is the relative displacement of building A to the base, x_B is the relative displacement of building B to the base, and $\ddot{y}_0$ is the ground input acceleration to the buildings.

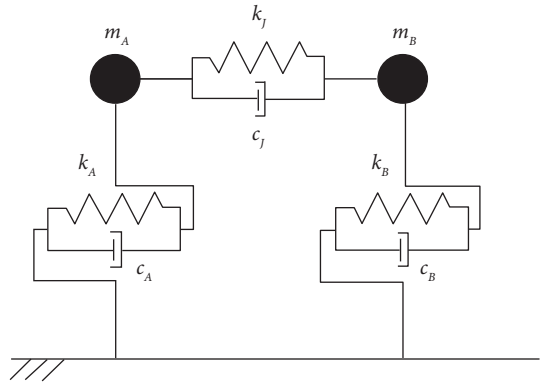

Figure 1: The 2-DOF model for joint damper.

A natural circular frequency and the corresponding damping ratio are defined for each S-DOF building model: ω_A and ω_B are the natural frequencies for building A and building B, respectively, and h_A and h_B are the corresponding damping ratios.

$$\begin{aligned} \omega_A^2 &= \frac{k_A}{m_A}, \\ \omega_B^2 &= \frac{k_B}{m_B}, \\ 2h_A\omega_A &= \frac{c_A}{m_A}, \\ 2h_B\omega_B &= \frac{c_B}{m_B}. \end{aligned} \tag{2}$$

Furthermore, μ is the mass ratio of building B to building A.

$$\mu = \frac{m_B}{m_A}. \tag{3}$$

For the joint damper, the natural circular frequency (ω_J) and damping ratio (h_J) are defined as follows:

$$\begin{aligned} \omega_J^2 &= \frac{k_J}{m_B}, \\ 2h_J\omega_B &= \frac{c_J}{m_B}. \end{aligned} \tag{4}$$

These definitions introduce the following relations:

$$\begin{aligned} \frac{k_J}{m_A} &= \frac{m_B}{m_A}\frac{k_J}{m_B} = \mu\omega_J^2, \\ \frac{c_J}{m_A} &= \frac{m_B}{m_A}\frac{c_J}{m_B} = 2\mu h_J\omega_B. \end{aligned} \tag{5}$$

Considering equations (2)–(5), the equation of motion (1) can be written as follows:

$$\begin{Bmatrix} \ddot{x}_A \\ \ddot{x}_B \end{Bmatrix} + \begin{bmatrix} 2h_A\omega_A + 2\mu h_J\omega_B & -2\mu h_J\omega_B \\ -2h_J\omega_B & 2h_B\omega_B + 2h_J\omega_B \end{bmatrix} \begin{Bmatrix} \dot{x}_A \\ \dot{x}_B \end{Bmatrix} + \begin{bmatrix} \omega_A^2 + \mu\omega_J^2 & -\mu\omega_J^2 \\ -\omega_J^2 & \omega_B^2 + \omega_J^2 \end{bmatrix} \begin{Bmatrix} x_A \\ x_B \end{Bmatrix} = -\begin{Bmatrix} 1 \\ 1 \end{Bmatrix} \ddot{y}_0. \tag{6}$$

This is transformed into the state equation, as follows:

$$\begin{Bmatrix} \ddot{x}_A \\ \ddot{x}_B \\ \dot{x}_A \\ \dot{x}_B \end{Bmatrix} = \begin{bmatrix} -2h_A\omega_A - 2\mu h_J\omega_B & 2\mu h_J\omega_B & -\omega_A^2 - \mu\omega_J^2 & \mu\omega_J^2 \\ 2h_J\omega_B & -2h_B\omega_B - 2h_J\omega_B & \omega_J^2 & -\omega_B^2 - \omega_J^2 \\ 1 & 0 & 0 & 0 \\ 0 & 1 & 0 & 0 \end{bmatrix} \begin{Bmatrix} \dot{x}_A \\ \dot{x}_B \\ x_A \\ x_B \end{Bmatrix} - \begin{Bmatrix} 1 \\ 1 \\ 0 \\ 0 \end{Bmatrix} \ddot{y}_0. \tag{7}$$

2.2. Characteristic Equations for Assigned Poles and 2-DOF System. Under practical circumstances, the 2-DOF model shown in Figure 1 has two sets of conjugate poles. When ω_j and h_j are defined as the natural circular frequency and damping ratio, respectively, in the j-th mode, the characteristic equation with the Laplace operator $s = i\omega$ (where ω is the circular frequency) is introduced, as follows:

$$\left(s^2 + 2h_1\omega_1 s + \omega_1^2\right)\left(s^2 + 2h_2\omega_2 s + \omega_2^2\right) = 0. \tag{8}$$

This equation can be rewritten in the following polynomial form:

$$\begin{aligned} s^4 + 2\left(h_1\omega_1 + h_2\omega_2\right)s^3 + \left(\omega_1^2 + 4h_1h_2\omega_1\omega_2 + \omega_2^2\right)s^2 \\ + 2\omega_1\omega_2\left(h_2\omega_1 + h_1\omega_2\right)s + \omega_1^2\omega_2^2 = 0. \end{aligned} \tag{9}$$

The characteristic equation for the state equation (7) is expressed as follows:

$$\begin{vmatrix} -2h_A\omega_A - 2\mu h_J\omega_B - s & 2\mu h_J\omega_B & -\omega_A^2 - \mu\omega_J^2 & \mu\omega_J^2 \\ 2h_J\omega_B & -2h_B\omega_B - 2h_J\omega_B - s & \omega_J^2 & -\omega_B^2 - \omega_J^2 \\ 1 & 0 & -s & 0 \\ 0 & 1 & 0 & -s \end{vmatrix} = 0. \tag{10}$$

When the four-dimensional full matrix A is divided into four two-dimensional submatrices A_{11}, A_{12}, A_{21}, and A_{22}, the following equation can be applied to obtain the determinant of equation (10):

$$|A| = \left|A_{22}\right|\left|A_{11} - A_{12}A_{22}^{-1}A_{21}\right|. \tag{11}$$

Consequently, this determinant can be expressed in the polynomial form as follows:

$$\begin{aligned} s^4 + 2\left\{h_A\omega_A + h_B\omega_B + (1+\mu)h_J\omega_B\right\}s^3 \\ + \left\{\omega_A^2 + \omega_B^2 + (1+\mu)\omega_J^2 + 4\left(h_Ah_B\omega_A\omega_B + h_Ah_J\omega_A\omega_B + \mu h_Bh_J\omega_B^2\right)\right\}s^2 \\ + 2\left\{h_A\omega_A\left(\omega_B^2 + \omega_J^2\right) + h_B\omega_B\left(\omega_A^2 + \mu\omega_J^2\right) + h_J\omega_B\left(\omega_A^2 + \mu\omega_B^2\right)\right\}s + \omega_A^2\omega_B^2 + \mu\omega_B^2\omega_J^2 + \omega_A^2\omega_J^2 = 0. \end{aligned} \tag{12}$$

2.3. Pole Allocation. Equation (12) must be designed to be equal to the target characteristic in equation (9), which requires satisfying the following parameter relationships:

$$h_A\omega_A + h_B\omega_B + (1+\mu)h_J\omega_B = h_1\omega_1 + h_2\omega_2, \tag{13}$$

$$\omega_A^2 + \omega_B^2 + (1+\mu)\omega_J^2 + 4\left(h_Ah_B\omega_A\omega_B + h_Ah_J\omega_A\omega_B + \mu h_Bh_J\omega_B^2\right) = \omega_1^2 + 4h_1h_2\omega_1\omega_2 + \omega_2^2, \tag{14}$$

$$h_A\omega_A\left(\omega_B^2 + \omega_J^2\right) + h_B\omega_B\left(\omega_A^2 + \mu\omega_J^2\right) + h_J\omega_B\left(\omega_A^2 + \mu\omega_B^2\right) = \omega_1\omega_2\left(h_2\omega_1 + h_1\omega_2\right), \tag{15}$$

$$\omega_A^2\omega_B^2 + \mu\omega_B^2\omega_J^2 + \omega_A^2\omega_J^2 = \omega_1^2\omega_2^2. \tag{16}$$

Dividing equation (15) by equation (16) yields the following expression:

$$\frac{h_A\omega_A\left(\omega_B^2+\omega_J^2\right)}{\omega_A^2\omega_B^2+\mu\omega_B^2\omega_J^2+\omega_A^2\omega_J^2}+\frac{h_B\omega_B\left(\omega_A^2+\mu\omega_J^2\right)}{\omega_A^2\omega_B^2+\mu\omega_B^2\omega_J^2+\omega_A^2\omega_J^2}+\frac{h_J\omega_B\left(\omega_A^2+\mu\omega_B^2\right)}{\omega_A^2\omega_B^2+\mu\omega_B^2\omega_J^2+\omega_A^2\omega_J^2}=\frac{h_1}{\omega_1}+\frac{h_2}{\omega_2}. \tag{17}$$

Substituting equations (2)–(5) into equation (17) yields the following expression:

$$\frac{1}{2}\left(\frac{c_A}{k_A+1/\left(1/k_B+1/k_J\right)}+\frac{c_B}{k_B+1/\left(1/k_A+1/k_J\right)}+\frac{c_J}{k_J+1/\left(1/k_A+1/k_B\right)}\right)=\frac{h_1}{\omega_1}+\frac{h_2}{\omega_2}. \tag{18}$$

The introduced equation automatically constrains the variations in the structural parameters under the assigned modal properties. For example, when the values on the right side and those of k_A, k_B, and k_J are fixed, the variations in c_A, c_B, and c_J are constrained.

On the left side, the denominators and numerators represent the equivalent stiffness and damping coefficients, respectively. This equation is similar to equation (19) for the 3-DOF damped model shown in Figure 2 [3, 4].

$$\frac{1}{2}\left(\frac{c_1}{k_1}+\frac{c_2}{k_2}+\frac{c_3}{k_3}\right)=\frac{h_1}{\omega_1}+\frac{h_2}{\omega_2}+\frac{h_3}{\omega_3}, \tag{19}$$

where k_i and c_i are the shear stiffness and damping coefficient, respectively, in the i-th story and ω_j and h_j are the natural circular frequency and damping ratio, respectively, in the j-th mode. Figure 3 shows the third term on the left side of equation (18). The denominator in the third term is the equivalent spring, where k_J is parallel to the combined springs of k_A and k_B in the series.

2.4. Closed Expression of the Optimum Damping for Joint Damper. The fixed-point theory optimizes the damping coefficient of a joint damper connecting two adjacent buildings [7]. This theory assumes a 2-DOF model wherein only a dashpot connects two S-DOF undamped models because, in general, the structural damping ratios are smaller than those of the dashpot. This assumption sets $c_A = c_B = k_J = 0$ in equation (1), which introduces the following expression:

$$\begin{Bmatrix}\ddot{x}_A\\ \ddot{x}_B\end{Bmatrix}+\begin{bmatrix}2\mu h_J\omega_B & -2\mu h_J\omega_B\\ -2h_J\omega_B & 2h_J\omega_B\end{bmatrix}\begin{Bmatrix}\dot{x}_A\\ \dot{x}_B\end{Bmatrix}+\begin{bmatrix}\omega_A^2 & 0\\ 0 & \omega_B^2\end{bmatrix}\begin{Bmatrix}x_A\\ x_B\end{Bmatrix}=-\begin{Bmatrix}1\\ 1\end{Bmatrix}\ddot{y}_0. \tag{20}$$

Notably, the spring k_J becomes unnecessary when the product of mass ratio μ and frequency ratio $\gamma = \omega_B/\omega_A$, in other words, the product of the mass ratio and stiffness ratio, is constant [11, 15, 16]. Furthermore, a spring is required only when the masses of the two models differ significantly, and the natural frequency of an S-DOF model with a smaller mass is lower than that of another S-DOF model with a larger mass.

The original theory was introduced using absolute coordinates, where the structural displacements included the base displacement [7]. In architectural engineering, base displacement is the ground displacement that cannot be controlled by dampers. Therefore, before pole allocation is applied to a joint damper for buildings, the absolute coordinates should be converted into relative coordinates, where the structural displacement is relative to the base. Appendix A introduces the fixed-point theory in the relative coordinates.

The optimal $h_{J,\mathrm{opt}}$ for the joint damper is defined as the average value using equations (A.29) and (A.30), which implies that the coordinate conversion does not affect the optimization.

$$h_{J,\mathrm{opt}}=\frac{|1-\mu|}{4(1+\mu)\sqrt{2(1+\mu)}}\left(2+\mu+\frac{1+2\mu}{\sqrt{\mu}}\right). \tag{21}$$

This closed expression plays a significant role when equation (18) is integrated with the fixed-point theory.

2.5. Integration of Governing Equation and the Fixed-Point Theory. Equation (18) and the early fixed-point theory are combined to produce a simple design method for a joint damper because the fixed-point theory provides not the structural damping effect but the optimum damping coefficient for the joint damper, and the equation expresses the relationship among all the structural parameters under the assigned modal damping ratios. This integration directly links the structural damping with the damping of the joint damper. As described in Subsection 2.4, the proposed fixed-point theory [7] assumes $c_A = c_B = k_J = 0$. This assumption leads to the following equation from Equation (18):

$$\frac{1}{2}\frac{c_J}{1/\left(1/k_A+1/k_B\right)}=\frac{1}{2}\frac{c_J}{k_Ak_B/\left(k_A+k_B\right)}=\frac{h_1}{\omega_1}+\frac{h_2}{\omega_2}. \tag{22}$$

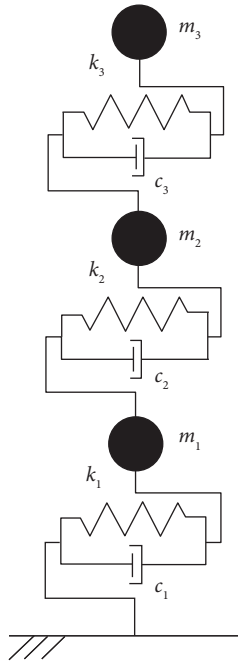

Figure 2: The 3-DOF model.

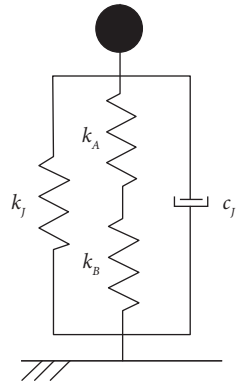

Figure 3: The equivalent S-DOF model for 3rd term on the left side of equation (18).

When $c_{J,\mathrm{opt}}$ is defined as the damping coefficient corresponding to $h_{J,\mathrm{opt}}$, equations (2)–(4) yield equations (23) and (24), respectively, as follows:

$$c_{J,\mathrm{opt}} = 2m_B\omega_B h_{J,\mathrm{opt}} = 2\mu\gamma m_A\omega_A h_{J,\mathrm{opt}}, \tag{23}$$

$$\frac{k_A k_B}{k_A + k_B} = \frac{\mu\gamma^2}{1+\mu\gamma^2} m_A\omega_A^2. \tag{24}$$

Substituting equations (23) and (24) in equation (22) yields the following expression:

$$\frac{1+\mu\gamma^2}{\gamma}\frac{h_{J,\mathrm{opt}}}{\omega_A} = \frac{h_1}{\omega_1} + \frac{h_2}{\omega_2}. \tag{25}$$

Numerous practical applications of structural control, excluding seismic isolation, have reported additional damping effect on buildings [32, 33]. From the viewpoint of equivalent damping, the authors in [32] summarized several reports on active and semiactive control and the authors in [33] summarized several reports on passive control during the 2011 Great Tohoku Earthquake. This study considered only the dashpot between two adjacent buildings, which primarily affects the additional damping of the two adjacent buildings. Therefore, this study focused on an additional damping effect. To provide two buildings with the same damping ratio ($h = h_1 = h_2$), equation (25) can be written as follows:

$$\frac{1+\mu\gamma^2}{\gamma}\frac{h_{J,\mathrm{opt}}}{\omega_A} = h\left(\frac{1}{\omega_1} + \frac{1}{\omega_2}\right). \tag{26}$$

Considering that both the buildings are connected by only a dashpot, the natural frequencies, ω_1 and ω_2, approximately equal ω_A and ω_B, respectively. It cannot be determined which vibration mode is responsible for building A or building B. However, this selection is not an issue in this formulation because the two S-DOF models are exchangeable in the 2-DOF model.

$$\frac{1+\mu\gamma^2}{\gamma}\frac{h_{J,\mathrm{opt}}}{\omega_A} = h\left(\frac{1}{\omega_A} + \frac{1}{\omega_B}\right), \tag{27}$$

$$h = \frac{1+\mu\gamma^2}{1+\gamma} h_{J,\mathrm{opt}}. \tag{28}$$

This equation shows the relationship between the optimal damping of the damper itself $h_{J,\mathrm{opt}}$ and the additional damping of the structure h. Using this equation, it is possible to directly estimate the damping of the structure from the damper damping. Substituting the optimum damping ratio from equations (21) into (28) yields the following expression:

$$h = \frac{\left(1+\mu\gamma^2\right)|1-\mu|}{4(1+\gamma)(1+\mu)\sqrt{2(1+\mu)}}\left(2+\mu+\frac{1+2\mu}{\sqrt{\mu}}\right). \tag{29}$$

The structural damping ratio h can be obtained by the mass ratio μ and frequency ratio γ. This is an advantage of integrating pole allocation and fixed-point theory. The authors in [7, 9–13] do not directly provide the control effectiveness.

3. Fundamental Characteristics via 2-DOF Model

Figure 4 shows the frequency transmissibilities of the two S-DOF buildings when μ is 0.8 and γ is 1.25. The solid lines represent building A, whereas the dashed lines represent building B. Here, h_J is 1%, 8.35%, and 50%. The optimum damping ratio $h_{J,\mathrm{opt}}$ is 8.35% when μ is 0.8. With h_J of 1%, the peaks for buildings A and B appear when ξ is 1.0 and 1.25. With h_J of 50%, two buildings are rigidly connected; consequently, the peaks appear when ξ is equal to 1.12, which is close to the average of 1.0 and 1.25. Fixed points P and Q are shown in the figure.

Figure 5 shows the relationship between μ and $h_{J,\mathrm{opt}}$, based on equations (A.29), (A.30), and (21). Although this study expresses the damper's optimum damping ratio in

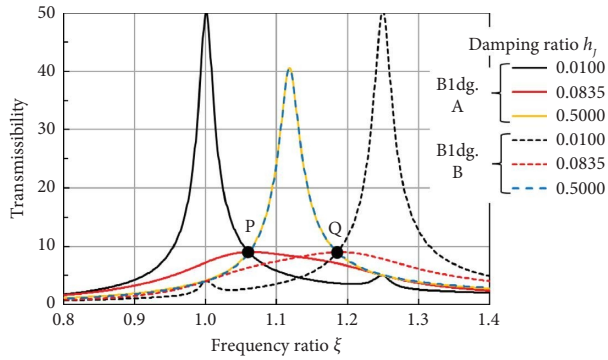

Figure 4: Frequency transmissibilities based on equations (A.2) and (A.3) ($\mu = 0.8$ and $\gamma = 1.25$).

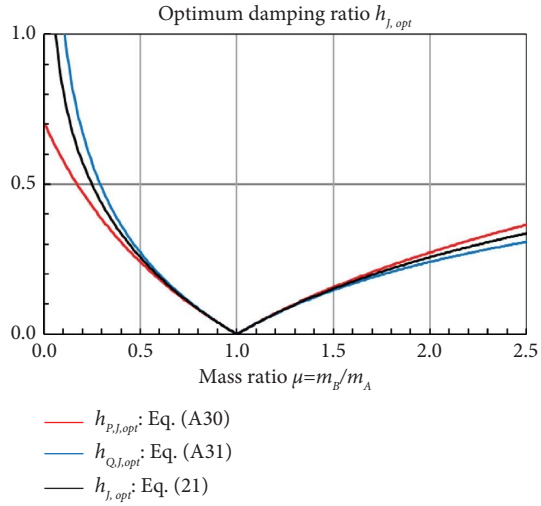

Figure 5: Optimum damping ratio $h_{J,\text{opt}}$ for joint damper.

a closed form, it is the same as that presented in [7]. For μ ranging from 0.5 to 2.5, equations (A.29) and (A.30) have a marginal difference, and the averaged equation (21) effectively approximates equations (A.29) and (A.30). When both masses are the same ($\mu = 1$), $h_{J,\text{opt}}$ approaches zero and the joint damper is unavailable.

Based on equation (29), Figure 6 shows the structural damping ratio h depending on μ and γ. When μ is the same, a higher frequency ratio increases the structural damping ratio. When μ is smaller, h is not significantly affected by γ. In general, the first natural frequency of a building is strongly affected by both the building height and structural materials, such as steel and reinforced concrete. If the materials of the two buildings are similar, the frequency ratio is close to unity for practical applications.

Figure 6 also shows the optimum damping ratio $h_{J,\text{opt}}$ for structural damping ratio h. The damping ratios h and $h_{J,\text{opt}}$ have the same scale, thus implying that the damper directly contributes to the control effect. This is because this damper can secure a large reaction using an adjacent building, as described in [11]. Equation (28) demonstrates this advantage.

4. Application of Equations (28) and (29) to Two M-DOF Models

Equations (28) and (29) are introduced based on the 2-DOF model, which considers only the first modes of both buildings. In this study, two adjacent buildings with almost the same height are passively controlled using a joint damper connected to the top floors. Consequently, the first modes of both buildings are controlled. When M-DOF models are used in the design, higher modes must be considered, even if only the first modes are the objectives. This section describes the application of equations (28) and (29) to M-DOF models.

4.1. Numerical Models. As shown in Figure 7, a 10-DOF shear model with ten lumped masses was first assumed to be building A. Table 1 lists the distributions of the lumped masses, shear stiffness values, and damping coefficients. The total mass was 5000×10^3 kg, and the damping coefficients were proportional to the corresponding stiffness matrix, which indicates internal viscous damping. The damping ratio of building A is 1% in the first mode.

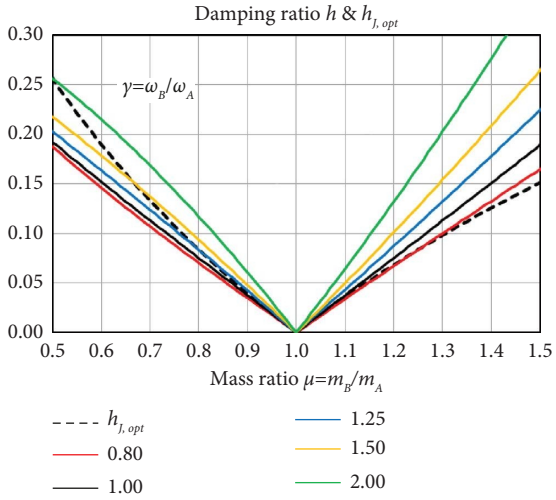

Figure 6: Structural damping ratio h in comparison to optimum damping ratio $h_{J,\mathrm{opt}}$ for joint damper.

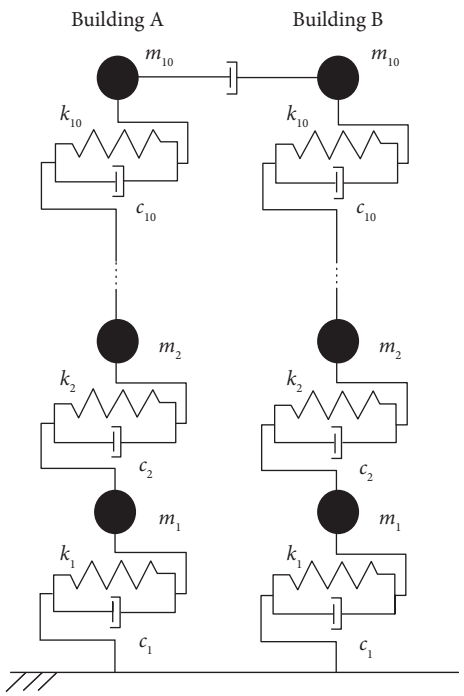

Figure 7: The 20-DOF model.

Table 1: Structural parameters for the model A.

Lumped mass no.	Mass (10^3 kg)	Story	Stiffness (MN/m)	Damping coefficient (MNs/m)
10	600	10	318.7	1.090
9	450	9	367.7	1.257
8	450	8	441.3	1.509
7	450	7	514.8	1.760
6	470	6	588.4	2.012
5	470	5	656.5	2.347
4	490	4	784.5	2.682
3	510	3	882.6	3.018
2	560	2	980.7	3.353
1	550	1	1078.7	3.688

In Japan, the initial damping ratio for the first vibration mode is assumed to be 1% for steel buildings or 3% for reinforced concrete buildings. The analytical 10-DOF model assumes a 10-story building, and the first natural frequencies are around 1 Hz. The model images a steel building. The proposed method can determine the damper's capacity after specifying the additional damping ratio. As a result, the initial structural damping does not directly affect the specification of the additional damping ratio. Table 2 lists the natural frequencies and corresponding damping ratios, and Figure 8 shows the three lowest mode shapes with the participation factors for the seismic input. This model is referred to as model A in the numerical examples.

The adjacent 10-DOF building is building B, and the four submodels are labelled models B1, B2, B3, and B4. Evidently from Table 3, these submodels have two total mass ratios and two frequency ratios in the first modes. The mass and stiffness distributions of the submodels are proportional to those of model A. Similarly, the damping ratio for each submodel is 1% in the first mode. For all submodels, Tables 4–6 present the distributions of the lumped masses, shear stiffness values, and damping coefficients. Table 7 lists the two pairs of natural frequencies. Evidently, the mode shapes of each submodel are similar to those of model A because the mass and stiffness distributions are similar to those of model A. A joint damper is installed as a dashpot between the top masses of the models A and B.

4.2. Optimum Damping Using First Effective Mass in Each Building. The optimum damping ratio and coefficient for the joint damper are calculated using equations (21) and (23), where equation (23) uses the first effective modal mass of each model. The effective mass indicated in equation (30) does not depend on normalizing the mode shapes, and the sum of all effective masses matches the total mass [34].

$$M_j = \frac{\left(\sum_{i=1}^{n} m_i u_{ij}\right)^2}{\sum_{i=1}^{n} m_i u_{ij}^2}, \tag{30}$$

where M_j is the j-th effective modal mass, m_i is the i-th lumped mass, u_{ij} is the j-th mode shape of the i-th lumped mass, and n is the total number of modes. For the 20-DOF model, $n = 10$. Table 8 lists the first effective modal mass, first natural frequency, and optimal damping coefficient of each joint damper.

4.3. Correction for Structural Damping Ratio. Even if a damper with the optimum damping coefficient calculated from the first mode information is installed in a 20-DOF model, it is effective for higher modes. This requires correcting the structural damping ratio in equations (28) and (29) to predict control effectiveness.

A viscous joint damper determines the relative velocity between the top lumped masses, which is expressed as the corresponding relative displacement in an eigenvalue problem. Currently, an undamped eigenvalue problem is applied to the 20-DOF model because only two 10-DOF submodels are connected by a dashpot. In the application, each 10-DOF model has 10 modes, which are completely

Table 2: Natural frequencies and modal damping ratios of the model A.

Mode no.	Natural frequency (Hz)	Damping ratio (%)
1	0.931	1.00
2	2.389	2.57
3	3.887	4.18
4	5.344	5.74
5	6.686	7.18
6	7.856	8.44
7	8.966	9.63
8	10.01	10.76
9	11.19	12.02
10	12.45	13.38

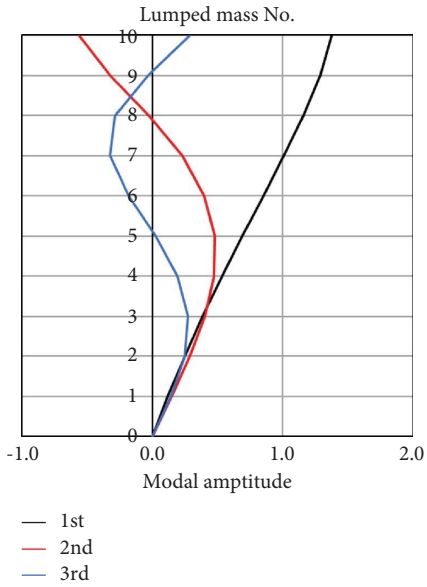

Figure 8: Mode shapes (model A).

Table 3: Total mass ratios and 1st frequency ratios for models B1, B2, B3, and B4.

Model	B1	B2	B3	B4
Mass ratio μ	0.9	1.1	0.9	1.1
Frequency ratio γ	1.25	1.25	0.80	0.80

Table 4: Lumped-mass distributions for models B1, B2, B3, and B4.

Lumped mass no.	B1 and B3 (10^3 kg)	B2 and B4 (10^3 kg)
10	540	660
9	405	495
8	405	495
7	405	495
6	423	517
5	423	517
4	441	539
3	459	561
2	504	616
1	495	605
Total mass	4500	5500
Mass ratio μ	0.9	1.1

Table 5: Stiffness distributions for models B1, B2, B3, and B4.

Story	B1 (MN/m)	B2 (MN/m)	B3 (MN/m)	B4 (MN/m)
10	448.2	547.8	183.6	224.4
9	517.1	632.1	211.8	258.9
8	620.6	758.5	254.2	310.7
7	724.0	884.9	296.6	362.5
6	827.4	1011.3	338.9	414.2
5	965.3	1179.9	395.4	483.3
4	1103.2	1348.4	451.9	552.3
3	1241.2	1517.0	508.4	621.3
2	1379.1	1685.5	564.9	690.4
1	1517.0	1854.1	621.3	759.4

Table 6: Damping distributions for models B1, B2, B3, and B4.

Story	B1 (MNs/m)	B2 (MNs/m)	B3 (MNs/m)	B4 (MNs/m)
10	1.226	1.498	0.785	0.959
9	1.414	1.728	0.905	1.106
8	1.697	2.074	1.086	1.328
7	1.980	2.420	1.267	1.549
6	2.263	2.766	1.448	1.770
5	2.640	3.226	1.690	2.065
4	3.017	3.687	1.931	2.360
3	3.394	4.148	2.173	2.655
2	3.771	4.609	2.414	2.951
1	4.148	5.070	2.655	3.246

Table 7: Natural frequencies of models B1, B2, B3, and B4.

Mode no.	B1 and B2 (Hz)	B3 and B4 (Hz)
1	1.164	0.745
2	2.986	1.911
3	4.859	3.110
4	6.680	4.275
5	8.357	5.348
6	9.820	6.285
7	11.21	7.173
8	12.52	8.011
9	13.99	8.951
10	15.57	9.963
Frequency ratio γ	1.25	0.80

independent of the others. As shown in Figure 9, the first and second modes of the 20-DOF model form a pair of first modes of the 10-DOF submodels and the third and fourth modes of the 20-DOF model form a pair of second modes of the 10-DOF submodels.

For each mode pair, the maximum relative displacement between the top masses is assumed as the sum of the absolute amplitudes of the corresponding modes. In the j-th mode of each 10-DOF submodel, the maximum relative displacement at the top masses is expressed as follows:

$$\left|u_{10j}^{A}\beta_{j}^{A}\right| + \left|u_{10j}^{B}\beta_{j}^{B}\right|, \tag{31}$$

where $u_{10j}^{A}\beta_{j}^{A}$ and $u_{10j}^{B}\beta_{j}^{B}$ are the j-th mode amplitudes considering the input participation at the top masses in models A and B, respectively. Figure 10 shows the contribution of the damper to each mode, as follows:

Table 8: First effective modal masses, first natural frequencies, and optimum damping coefficients for joint dampers.

Model	A	B1	B2	B3	B4
Effective modal mass M_1 (10^3 kg)	3771	3394	4148	3394	4148
Mass ratio μ	—	0.9	1.1	0.9	1.1
Optimum damp. ratio $h_{J,\text{opt}}$ (%)	—	3.95	3.57	3.95	3.57
Natural frequency f_1 (Hz)	—	1.164	1.164	0.745	0.745
Frequency ratio γ	—	1.25		0.80	
Optimum damping coefficient $c_{J,\text{opt}}$ (MNs/m)	—	1.961	2.168	1.254	1.387

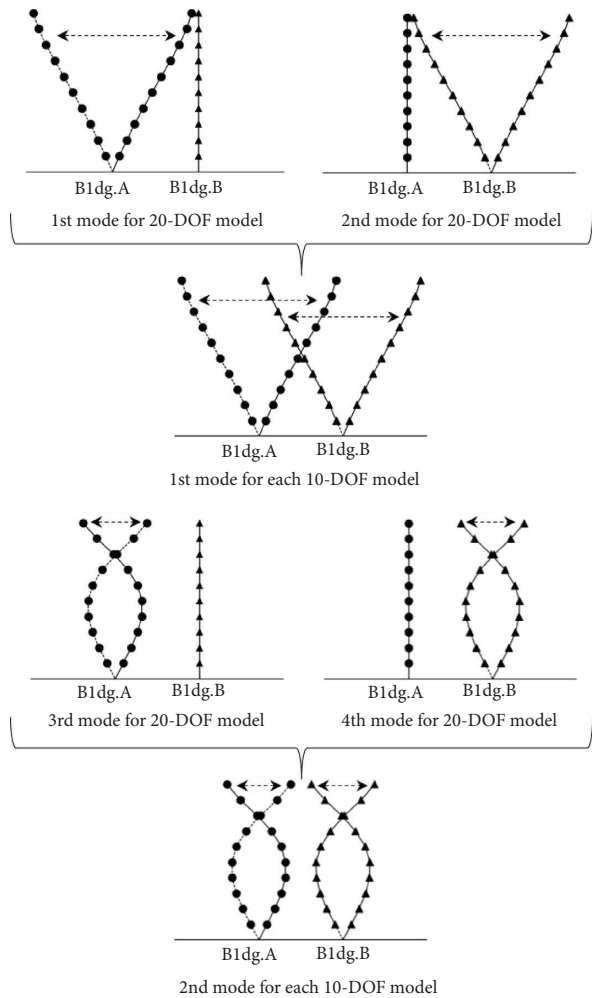

Figure 9: Modes (1^{st}–4^{th}) for the 20-DOF model.

$$\frac{\left|u_{10j}^{A}\beta_j^{A}\right| + \left|u_{10j}^{B}\beta_j^{B}\right|}{\sum_{j=1}^{10}\left(\left|u_{10j}^{A}\beta_j^{A}\right| + \left|u_{10j}^{B}\beta_j^{B}\right|\right)}. \tag{32}$$

In Figure 10, A1 is the contribution of the first mode in the model A and B2 is the contribution to the second mode in the model B. The sum of A1 and B1 (54.6%) represents the first-mode contributions of the 10-DOF submodels to the global 20-DOF model, whereas the sum of A2 and B2 (22.4%) represents the second-mode contributions of the 10-DOF submodels. The A1 contribution is similar to the B1 contribution, and the A2 contribution is similar to the B2 contribution because all the building models have similar mode shapes. In the higher modes, the mode contributions decrease. Figure 10 indicates that the damper works for higher modes even if the optimum damping coefficient is calculated from the first mode information. Essentially, 45.4% (100.0%–54.6%) damper capacity is used for the higher modes. Therefore, an increase of 1.83 (1.000/0.546) times was proposed as the optimum damping coefficient, as listed in Table 8.

Subsequently, the proposed increase procedure, which is a correction, is verified using the poles of the system matrix of each 20-DOF model. Table 8 lists the optimum damping coefficients installed in each 20-DOF model, and Table 9 lists the

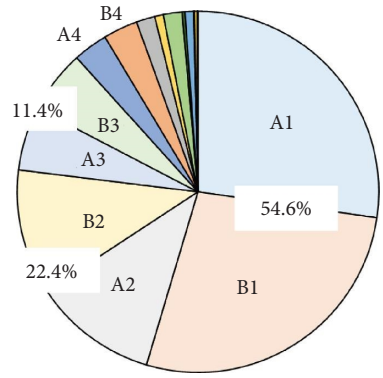

Figure 10: Joint damper contribution to each mode.

additional damping ratios in the first mode of each 10-DOF model by the joint damper. The additional damping ratios are defined as the difference from the initial damping ratio of 1% for the 10-DOF models. The damping ratio of the model B differs from that of the model A. The average ratio is compared with the value predicted using equation (28). In models A-B1, the additional damping ratios are 8.14% for building A and 8.01% for building B, with an average of 8.07%. The average value is 1.91 times 4.22%, which is predicted using equation (28) for the 2-DOF model. Furthermore, the average ratio of the 20-DOF model to the 2-DOF model is 1.89, which aligns with the value of 1.83, as shown in Figure 10. Equation (28) links the damping coefficient of the damper to additional structural damping ratio. An increase of 1.83 times implies that the predicted structural damping ratio should increase proportionally. To predict the control effectiveness for both M-DOF buildings, the additional damping ratios from Equations (28) and (29) should be updated by considering the mode contribution.

Based on the optimization of the joint damper through the fixed-point theory, this study proposed a simple method to predict additional structural damping without dynamic analysis. This introduces an assumption that equally considers the maximum relative displacements with input participation effects in all modes. Although Table 9 indicates that this assumption is acceptable at the preliminary design stage, a theoretical approach may be required in the future.

4.4. Verification via Seismic Response Analyses. In general, the fixed-point theory and the pole allocation method cannot predict structural response, damper's stroke, and damping force under a seismic excitation, because the fixed-point theory shapes the frequency transfer functions and the pole allocation method assigns the system's poles. All the responses including the stroke and damping force depend on dynamic nature of earthquakes. However, the pole allocation method has an advantage that the system's poles are independent of seismic nature, which can make the preliminary design easier. The seismic response analyses are needed to know the structural and damper's responses.

The seismic response analyses input the 1940 El Centro wave (NS component) and the 1952 Taft wave (EW component) into the four 20-DOF models described in Section 4.1. The inputs excite them sufficiently because the first natural frequencies of the models range from 0.745 to 1.164 Hz. The input amplitude is normalized such that the peak velocity is 25 cm/s. The corresponding peak accelerations are 255.5 cm/s^2 for El Centro and 248.4 cm/s^2 for Taft. This normalization scale assumes that the pole allocation can be applied to linear or equivalent linear systems. Figures 11–14 show the structural responses under the El Centro excitation.

Figure 11 shows the peak response distributions when model A is connected to model B1, referred to as models A-B1. Figure 11(a) shows the response accelerations at the lumped masses; Figures 11(b) and 11(c) show the response velocities and displacements to the base, respectively; and Figure 11(d) shows the corresponding response interstory displacements. The two dashed lines represent the uncontrolled responses when the two 10-DOF models are not connected, whereas the two solid lines represent the controlled responses of the 20-DOF model. Black represents model A, whereas red represents model B1. The optimum damping coefficient for the damper $c_{J,\mathrm{opt}}$ is 1.961 MNs/m, as listed in Table 8. The damping ratios in the first mode are 9.14% and 9.01% for models A and B1, respectively. The additional damping ratios of 8.14% and 8.01% in Table 9 differ from those for an initial structural damping ratio of 1%. At lumped mass no. 7 in Figure 11(b), the controlled velocity slightly exceeds the uncontrolled velocity in model A, and the overall control effectiveness is evident. In Figures 11(a) and 11(b), the uncontrolled responses differ in both buildings, whereas the controlled responses are similar.

Figure 12 depicts the peak response distribution for models A-B2. The response distributions are almost the same as those of models A-B1 because its frequency ratio γ is 1.25, similar to that of models A-B1. In both the models, the response reduction effectiveness of building B is higher than that of building A. It is relatively easy for a joint damper to reduce uncontrolled responses to the same level.

Figures 13 and 14 show the peak response distributions for models A-B3 and models A-B4, respectively. In building A, all controlled responses are smaller than the uncontrolled responses, whereas in building B, the controlled responses are close to the uncontrolled responses, and certain controlled velocities and displacements are slightly larger than the uncontrolled responses. The response distributions of models A-B4 are almost the same

Table 9: Comparison of damping ratios in the first modes.

Model for building B	Damping ratio by equation (28) (%)	*Additional damping ratio in the 1st mode (%)*			Average/equation (28)
		Building A	Building B	Average	
B1	4.22	8.14	8.01	8.07	1.91
B2	4.32	9.42	6.72	8.07	1.87
B3	3.46	5.48	7.52	6.50	1.88
B4	3.38	6.19	6.67	6.43	1.90
Average					1.89

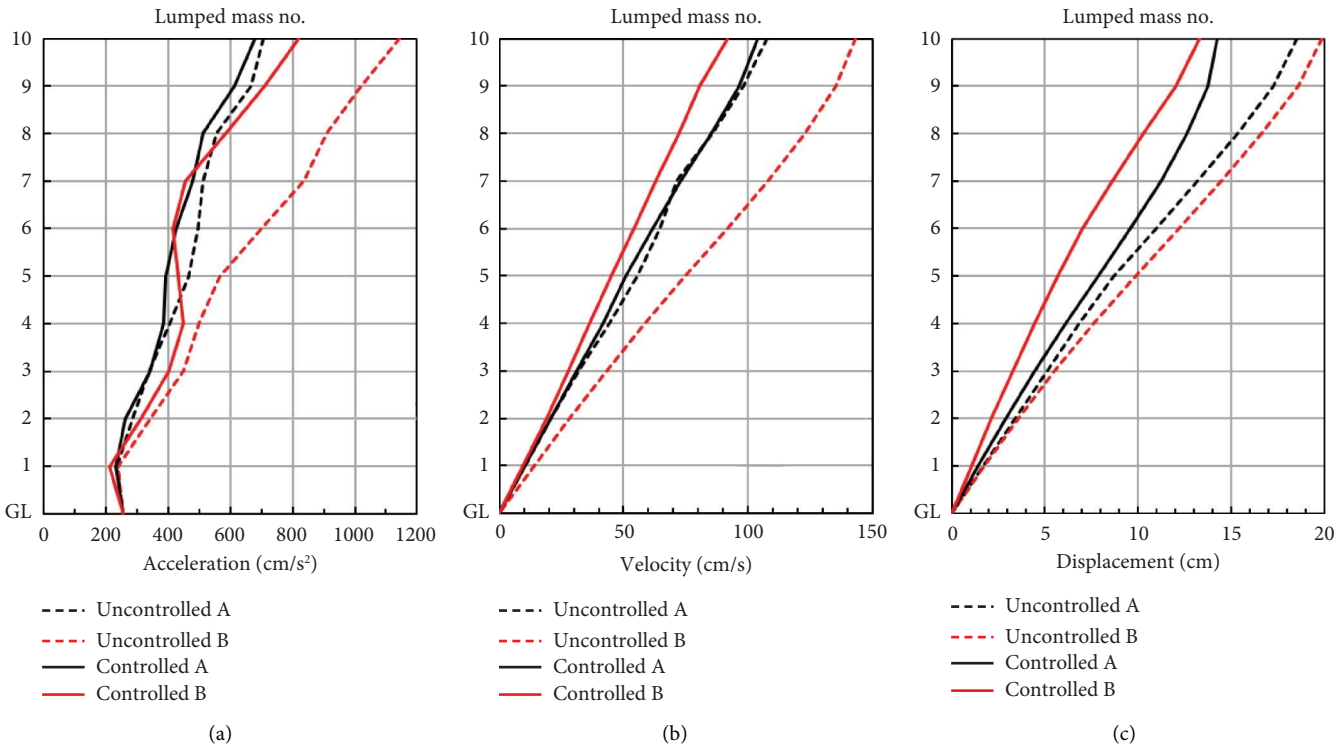

Figure 11: Continued.

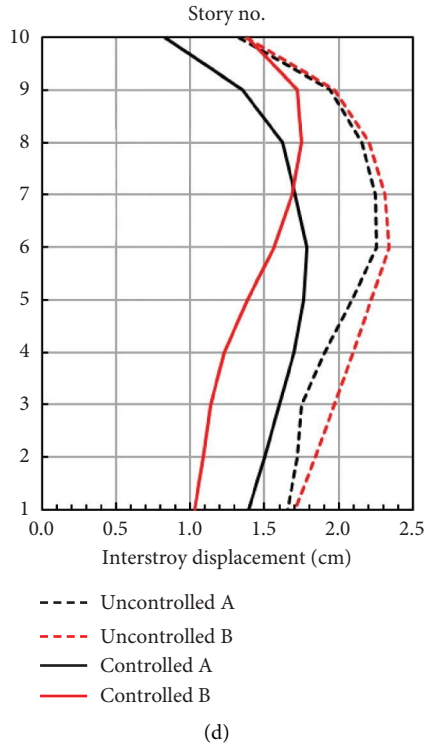

Figure 11: Peak response distributions of models A-B1 under El Centro excitation. (a) Acceleration. (b) Velocity. (c) Displacement. (d) Interstory displacement.

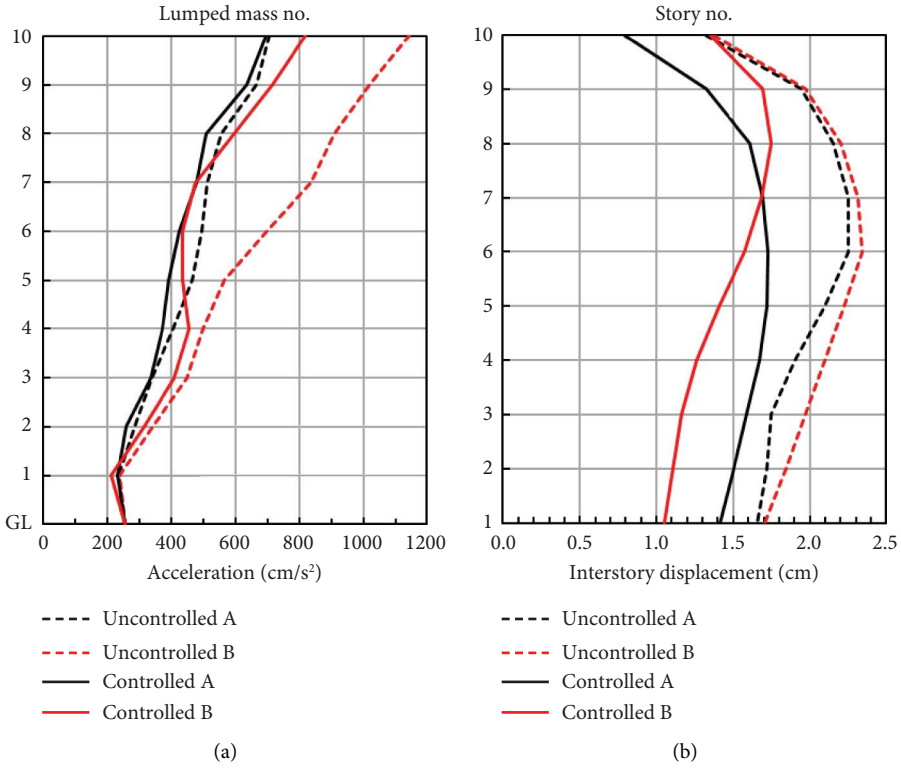

Figure 12: Peak response distributions of models A-B2 under El Centro excitation. (a) Acceleration. (b) Interstory displacement.

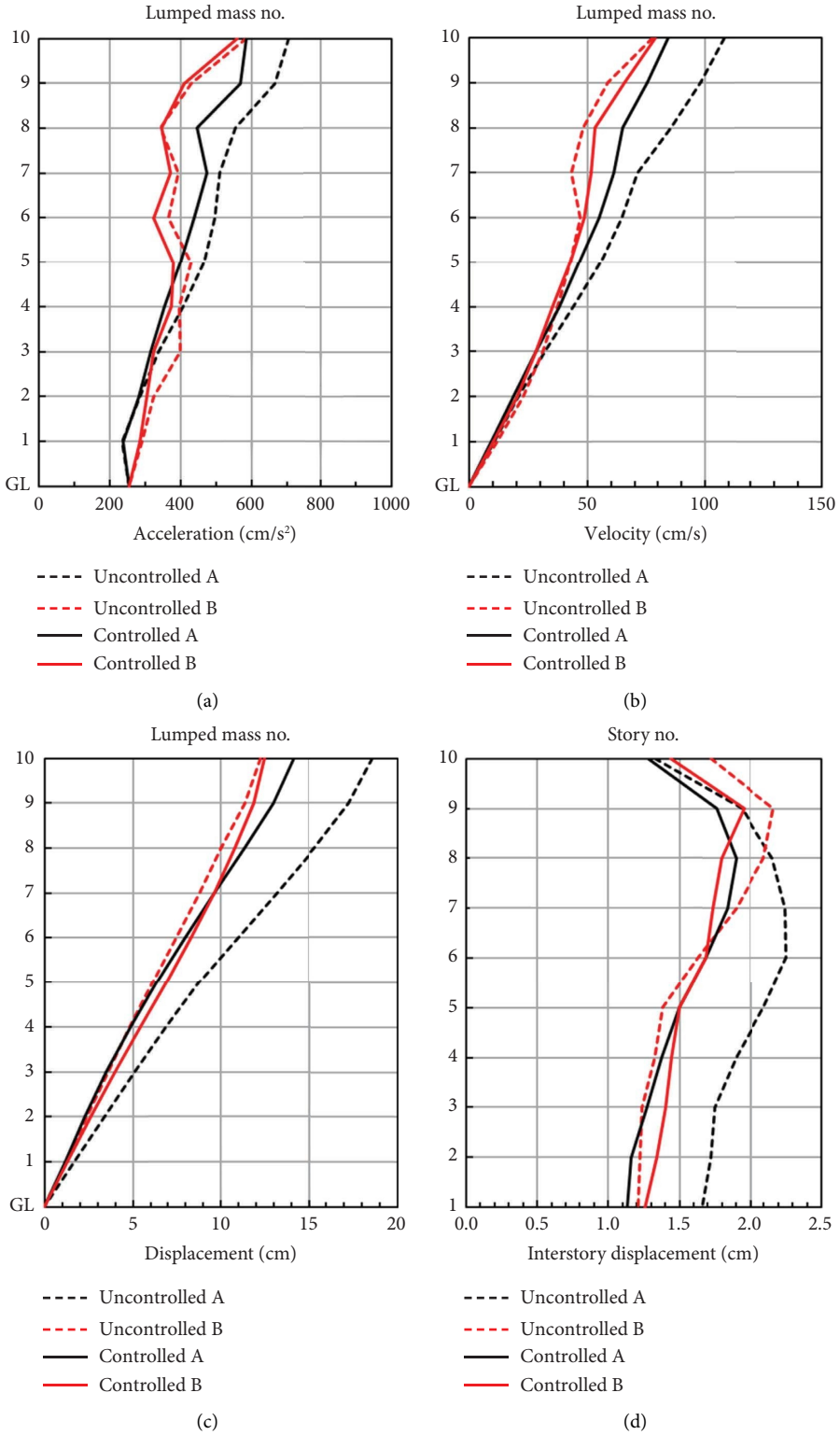

Figure 13: Peak response distributions of models A-B3 under El Centro excitation. (a) Acceleration. (b) Velocity. (c) Displacement. (d) Interstory displacement.

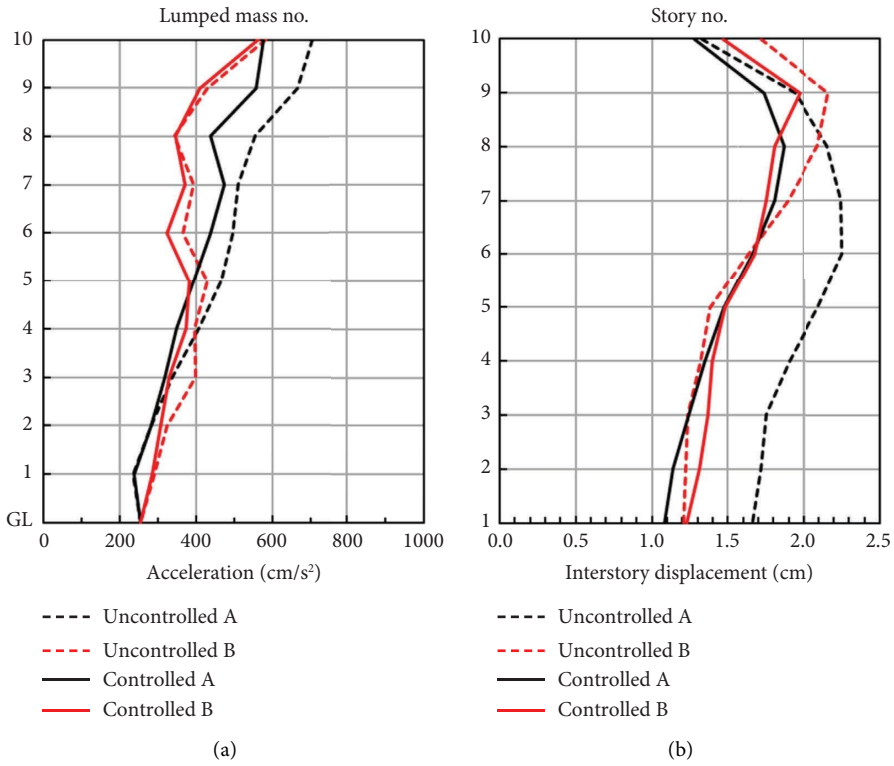

Figure 14: Peak response distributions of models A-B4 under El Centro excitation. (a) Acceleration. (b) Interstory displacement.

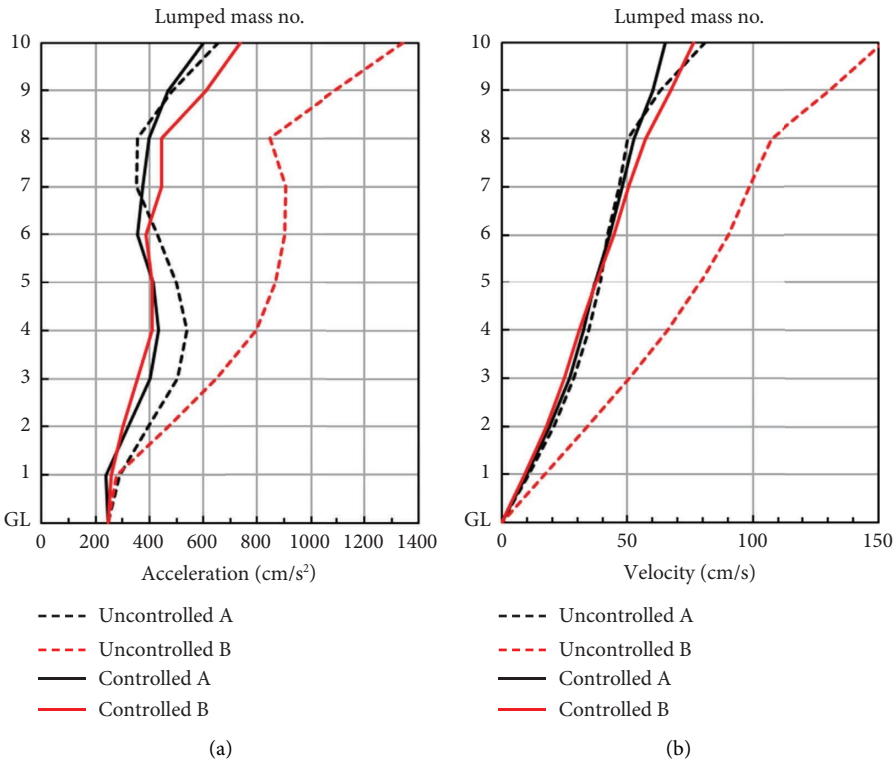

Figure 15: Continued.

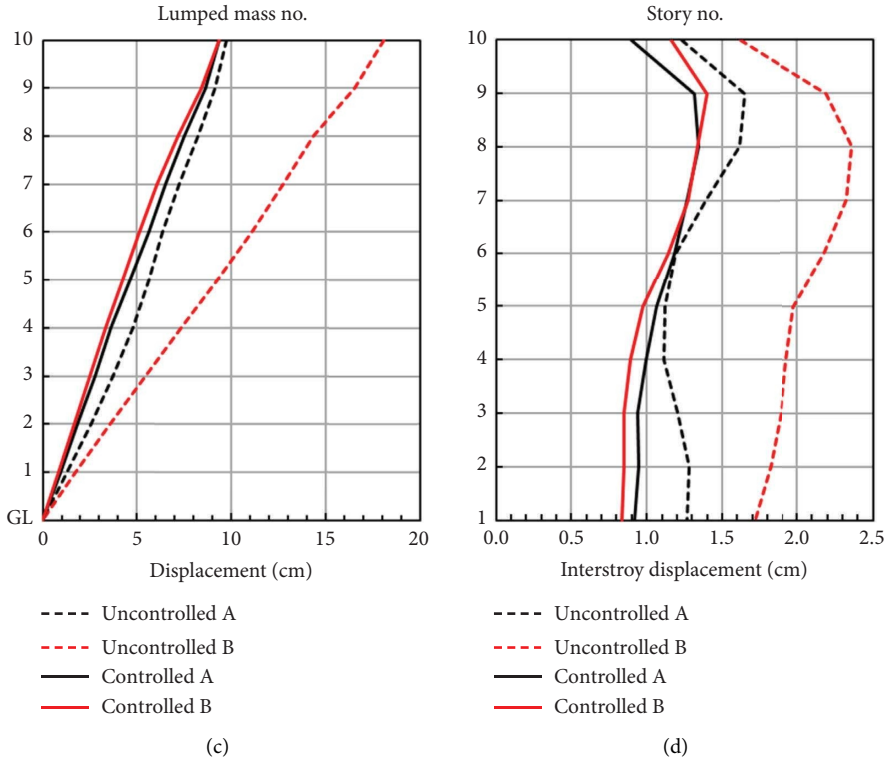

Figure 15: Peak response distributions of models A-B1 under Taft excitation. (a) Acceleration. (b) Velocity. (c) Displacement. (d) Interstory displacement.

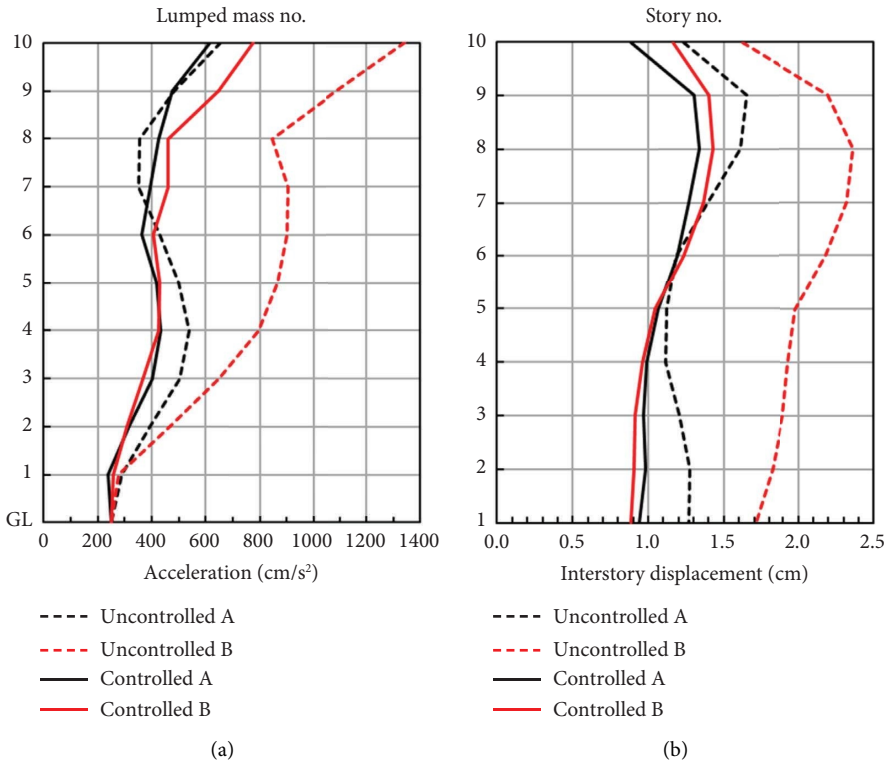

Figure 16: Peak response distributions of models A-B2 under Taft excitation. (a) Acceleration. (b) Interstory displacement.

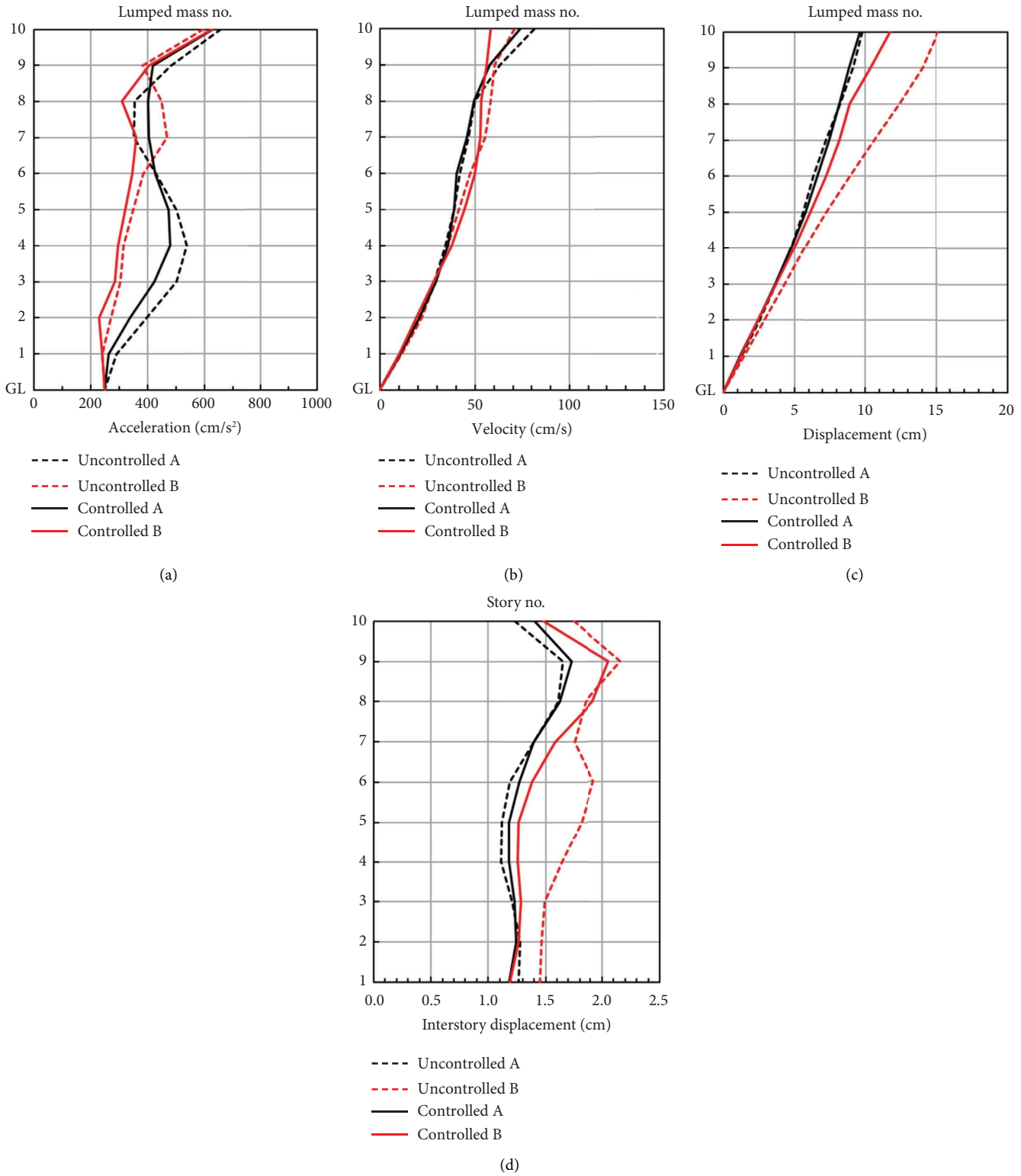

Figure 17: Peak response distributions of models A-B3 under Taft excitation. (a) Acceleration. (b) Velocity. (c) Displacement. (d) Interstory displacement.

as those of models A-B3 because its frequency ratio γ is 0.80, similar to that of models A-B3. The tendencies observed in Figures 13 and 14 are similar to those in Figures 11 and 12, respectively.

Equations (28) and (29) provide the two buildings with the same additional damping ratio. Although this intention was almost achieved, as presented in Table 9, the controlled responses are slightly larger than the uncontrolled responses

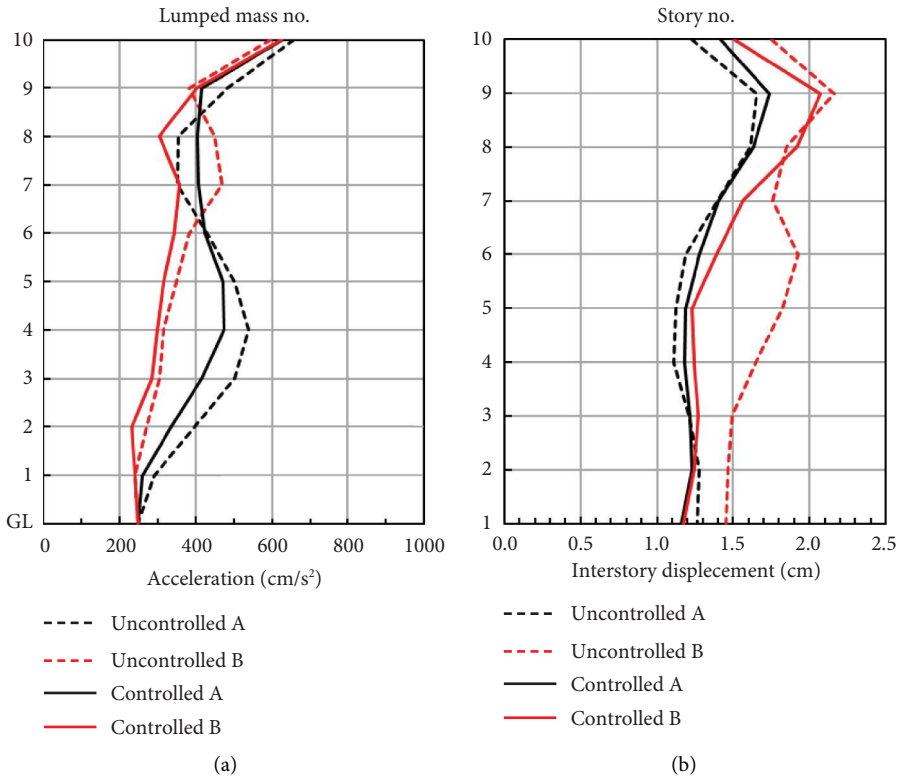

Figure 18: Peak response distributions of models A-B4 under Taft excitation. (a) Acceleration. (b) Interstory displacement.

Table 10: Peak strokes and peak damping forces of joint dampers.

Excitation	*El Centro*				*Taft*			
Models	A-B1	A-B2	A-B3	A-B4	A-B1	A-B2	A-B3	A-B4
Stroke (cm)	13.7	13.6	13.4	13.0	8.1	8.1	11.8	11.7
Damping force (kN)	1978	2195	1004	1078	1395	1574	916	1021

Table 11: Peak accelerations under El Centro excitation.

Model	*A-B1*		*A-B2*		*A-B3*		*A-B4*	
Building mass no.	Uncontrolled	Controlled	Uncontrolled	Controlled	Uncontrolled	Controlled	Uncontrolled	Controlled
A-10	705.3	680.0	705.3	696.4	705.3	584.7	705.3	577.5
A-9	666.2	613.7	666.2	636.6	666.2	567.5	666.2	557.3
A-8	554.4	510.6	554.4	507.7	554.4	445.9	554.4	439.1
A-7	511.5	480.0	511.5	478.8	511.5	474.6	511.5	475.7
A-6	496.3	426.8	496.3	426.5	496.3	438.7	496.3	438.9
A-5	466.1	390.5	466.1	391.1	466.1	400.3	466.1	393.7
A-4	406.2	383.7	406.2	370.4	406.2	355.2	406.2	349.5
A-3	337.4	340.6	337.4	333.5	337.4	316.6	337.4	317.7
A-2	283.5	260.7	283.5	258.5	283.5	283.3	283.5	283.3
A-1	235.2	232.6	235.2	232.3	235.2	238.3	235.2	238.6
B-10	1143.0	818.0	1143.0	818.7	584.3	561.8	584.3	563.7
B-9	1021.0	709.7	1021.0	716.0	429.0	410.1	429.0	411.0
B-8	908.1	587.2	908.1	595.0	344.7	347.0	344.7	345.0
B-7	836.1	454.4	836.0	473.9	394.1	370.0	394.1	371.0
B-6	700.5	415.3	700.5	433.8	365.3	323.1	365.3	323.1
B-5	566.0	432.0	566.0	434.4	430.0	378.7	430.0	383.4
B-4	497.3	449.9	497.3	454.0	395.2	373.8	395.2	375.5
B-3	447.6	402.9	447.6	406.9	398.7	324.2	398.7	330.8
B-2	340.5	312.4	340.5	314.7	323.3	305.5	323.3	307.1
B-1	236.5	210.5	236.5	211.8	291.6	283.7	291.6	284.4

Table 12: Peak displacements relative to the base under El Centro excitation.

Model	*A-B1*		*A-B2*		*A-B3*		*A-B4*	
Building mass no.	Uncontrolled	Controlled	Uncontrolled	Controlled	Uncontrolled	Controlled	Uncontrolled	Controlled
A-10	18.56	14.27	18.56	13.89	18.56	14.13	18.56	13.92
A-9	17.26	13.73	17.26	13.40	17.26	12.95	17.26	12.74
A-8	15.36	12.64	15.36	12.38	15.36	11.32	15.36	11.14
A-7	13.21	11.22	13.21	11.04	13.21	9.60	13.21	9.43
A-6	10.96	9.58	10.96	9.48	10.96	7.94	10.96	7.79
A-5	8.71	7.83	8.71	7.77	8.71	6.35	8.71	6.21
A-4	6.86	6.11	6.86	6.08	6.86	4.88	6.86	4.77
A-3	5.12	4.45	5.12	4.46	5.12	3.51	5.12	3.43
A-2	3.38	2.89	3.38	2.90	3.38	2.28	3.38	2.20
A-1	1.66	1.40	1.66	1.41	1.66	1.13	1.66	1.08
B-10	19.89	13.33	19.89	13.34	12.26	12.46	12.26	12.40
B-9	18.58	12.02	18.58	12.06	11.36	11.84	11.36	11.72
B-8	16.66	10.32	16.66	10.46	10.03	10.81	10.03	10.64
B-7	14.47	8.64	14.47	8.78	8.77	9.60	8.77	9.40
B-6	12.17	7.04	12.17	7.21	7.45	8.29	7.45	8.08
B-5	9.84	5.70	9.84	5.84	6.09	6.88	6.09	6.70
B-4	7.62	4.45	7.62	4.54	4.85	5.44	4.85	5.30
B-3	5.52	3.25	5.52	3.32	3.62	4.00	3.62	3.90
B-2	3.55	2.12	3.55	2.16	2.41	2.59	2.41	2.54
B-1	1.71	1.03	1.71	1.05	1.21	1.25	1.21	1.23

at some locations in some models. However, the controlled responses in both the models are almost identical. As described in the Introduction, a joint damper experiences difficulty in reducing uncontrolled responses with a certain reduction ratio. This difficulty has already been observed in seismic response analyses where two buildings with different heights are controlled passively or semiactively using magnetorheological dampers [35].

Figures 15–18 show the similar responses under the Taft excitation. In Figure 15, the uncontrolled responses differ in both buildings, whereas the controlled responses are similar. Figure 16 depicts the peak response distribution for models A-B2. The response distributions are almost the same as those of models A-B1 in Figure 15, because its frequency ratio γ is 1.25, similar to that of models A-B1. Figures 17 and 18 show the peak response distributions for models A-B3 and models A-B4, respectively. The response distributions of models A-B4 are almost the same as those of models A-B3 because of the similar frequency ratio. Under the Taft excitation, it is also confirmed that a joint damper easily reduces uncontrolled responses to the same level, and certain controlled responses are slightly larger than the uncontrolled responses even if two buildings have the same additional damping ratio.

Table 10 indicates strokes and damping forces by the joint dampers responding to Figures 11–18. Similar to the structural responses, the strokes and the damping forces depend on the dynamic nature of earthquakes.

5. Conclusion

For two adjacent buildings with a joint damper, an inverse problem was formulated based on the pole allocation method. The structural system was simplified as a 2-DOF model, wherein two S-DOF-damped models were connected by the damper. The unified governing equation, which expresses the relationship between an assigned control target and the structural parameters for an M-DOF shear building model, was extended to two buildings passively controlled by a joint damper. The governing equation was integrated with the fixed-point theory to directly estimate the additional damping effect on both buildings based on the capacity of the joint damper; this helps improve the past trial-and-error work at the preliminary design stage. The integration was verified using numerical examples of a 20-DOF building model, in which two 10-DOF models were connected by a damper between the top lumped masses. The results of this study are summarized as follows:

(1) The pole allocation method revealed a unified governing equation in the 2-DOF model, wherein two S-DOF damped models are connected by a joint damper. The equation automatically constrains the variations in the structural parameters under the assigned modal properties and similarly expresses the tradeoff relationship among the structural parameters under the controlled modal target, including the joint damper capacity.

(2) For building applications, the previously proposed fixed-point theory for joint dampers was rewritten in a closed form by converting the absolute coordinates into relative coordinates. The coordinate conversion interchanges two mathematical equations that express the optimum damping coefficients for the damper at two fixed points. However, the final optimum damping coefficient in the relative coordinates was similar to that in the absolute coordinates because the fixed-point theory adopts the average of the two optimum damping coefficients.

(3) The governing equation extended to the joint damper was integrated with fixed-point theory. In contrast to the fixed-point theory, the integration can

express the structural additional damping ratio of two adjacent buildings in a closed form and clearly indicates the relationship between the damper capacity and additional damping ratio. The control effectiveness depended on both the mass and frequency ratios of the two buildings, which did not necessitate that the two complex eigenvalues coincide. The closed-form expression improves the trial-and-error design of joint dampers at the preliminary design stage. The additional structural damping ratio had the same scale as the damping ratio of the damper, thus indicating that the joint damper worked effectively for structural control. A closed-form expression can contribute to a deeper physical understanding of the dynamic properties of joint dampers.

(4) The proposed prediction equation for the damping effect of the 2-DOF model was applied to two adjacent M-DOF buildings. A damper with an optimum damping coefficient, calculated from the first-mode information installed in the M-DOF model, was determined to be effective for higher modes. This required a correction for the structural damping ratio in the prediction of the control effectiveness. A correction method was proposed by considering the mode contributions based on the modal shapes, and it was verified through the damping ratios of the 20-DOF models. Although the correction method was verified in eigenvalue problems, a theoretical approach is required.

(5) The prediction equation for the damping effect was also studied in the seismic response analyses of 20-DOF models. Although the additional damping ratios and controlled seismic responses were almost identical for the two buildings, the response reduction rates differed in the two buildings. This result confirms that a joint damper experiences difficulty in reducing the uncontrolled responses at a certain reduction ratio.

Appendix

A. Fixed-Point Theory in Relative Coordinates

When both buildings are excited by a harmonic ground motion with a circular frequency ω, the ground displacement can be defined as $y = Y\exp(i\omega t)$ and the structural responses as $x_A = X_A\exp(i\omega t)$ and $x_B = X_B\exp(i\omega t)$. Furthermore, equation (20) can be expressed in the frequency domain, as follows:

$$\begin{bmatrix} \omega_A^2 - \omega^2 + 2i\mu h_J\omega_B\omega & -2i\mu h_J\omega_B\omega \\ -2ih_J\omega_B\omega & \omega_B^2 - \omega^2 + 2ih_J\omega_B\omega \end{bmatrix}\begin{Bmatrix} X_A \\ X_B \end{Bmatrix} = \omega^2\begin{Bmatrix} Y \\ Y \end{Bmatrix}. \tag{A.1}$$

The corresponding transmissibilities are as follows:

$$\left|\frac{X_A}{Y}\right| = \sqrt{\frac{\left(\gamma^2 - \xi^2\right)^2\xi^4 + 4h_J^2\gamma^2\xi^6(1+\mu)^2}{\left(1-\xi^2\right)^2\left(\gamma^2-\xi^2\right)^2 + 4h_J^2\gamma^2\xi^2\left\{1+\mu\gamma^2-(1+\mu)\xi^2\right\}^2}}, \tag{A.2}$$

$$\left|\frac{X_B}{Y}\right| = \sqrt{\frac{\left(1 - \xi^2\right)^2\xi^4 + 4h_J^2\gamma^2\xi^6(1+\mu)^2}{\left(1-\xi^2\right)^2\left(\gamma^2-\xi^2\right)^2 + 4h_J^2\gamma^2\xi^2\left\{1+\mu\gamma^2-(1+\mu)\xi^2\right\}^2}}, \tag{A.3}$$

where

$$\xi = \frac{\omega}{\omega_A}, \qquad \gamma = \frac{\omega_B}{\omega_A}. \tag{A.4}$$

These transmissibilities have two fixed points independent of h_J. The existence conditions for these fixed points for buildings A and B are, respectively, expressed as follows:

$$\begin{aligned} \left(1-\xi^2\right)^2\left(\gamma^2-\xi^2\right)^2 &: \left(\gamma^2-\xi^2\right)^2\xi^4 = 4h_J^2\gamma^2\xi^2\left\{1+\mu\gamma^2-(1+\mu)\xi^2\right\}^2 : 4h_J^2\gamma^2\xi^6(1+\mu)^2, \\ \left(1-\xi^2\right)^2\left(\gamma^2-\xi^2\right)^2 &: \left(1-\xi^2\right)^2\xi^4 = 4h_J^2\gamma^2\xi^2\left\{1+\mu\gamma^2-(1+\mu)\xi^2\right\}^2 : 4h_J^2\gamma^2\xi^6(1+\mu)^2. \end{aligned} \tag{A.5}$$

With physical meaning, these equations can be transformed into the following expression.

For building A,

$$\xi^2 = \frac{2+\mu+\mu\gamma^2}{2(1+\mu)}. \tag{A.6}$$

For building B,

$$\xi^2 = \frac{1+\gamma^2+2\mu\gamma^2}{2(1+\mu)}. \tag{A.7}$$

Because the fixed points are independent of h_J, the transmissibility at these points can be expressed as follows.

For building A,

$$\left|\frac{X_A}{Y}\right|_{h_J=0} = \sqrt{\frac{\xi^4}{\left(1-\xi^2\right)^2}}. \tag{A.8}$$

For building B,

$$\left|\frac{X_B}{Y}\right|_{h_J=0} = \sqrt{\frac{\xi^4}{\left(\gamma^2-\xi^2\right)^2}}. \tag{A.9}$$

Substituting equation (A.6) into (A.8) yields equation (A.10) and substituting equation (A.7) into (A.9) yields equation (A.11), as follows.

For building A,

$$\left|\frac{X_A}{Y}\right|_{h_J=0} = \frac{\xi^2}{1-\xi^2} = \pm\frac{2+\mu+\mu\gamma^2}{\left(1-\gamma^2\right)\mu}. \tag{A.10}$$

For building B,

$$\left|\frac{X_B}{Y}\right|_{h_J=0} = \frac{\xi^2}{\gamma^2-\xi^2} = \pm\frac{1+\gamma^2+2\mu\gamma^2}{\gamma^2-1}. \tag{A.11}$$

Both the fixed points have the same transmissibility:

$$\frac{2+\mu+\mu\gamma^2}{\left(1-\gamma^2\right)\mu} = \pm\frac{1+\gamma^2+2\mu\gamma^2}{\gamma^2-1}. \tag{A.12}$$

Based on a physical understanding, the selection of the positive sign in equation (A.12) results in the following expression:

$$\gamma = \frac{\omega_B}{\omega_A} = \frac{1}{\mu}. \tag{A.13}$$

This condition is similar to that indicated in [7], which implies that it is independent of the selected coordinates.

Substituting equation (A.13) into equations (A.10) and (A.11) yields the same transmissibility at the fixed points, which is expressed as follows.

For building A,

$$\left|\frac{X_A}{Y}\right|_P = \left|\frac{\xi^2}{1-\xi^2}\right| = \left|\frac{\mu+1}{\mu-1}\right|. \tag{A.14}$$

For building B,

$$\left|\frac{X_B}{Y}\right|_Q = \left|\frac{\xi^2}{\gamma^2-\xi^2}\right| = \left|\frac{\mu+1}{\mu-1}\right|. \tag{A.15}$$

Substituting equation (A.13) into equations (A.6) and (A.7) yields the nondimensional frequencies at the fixed points P and Q, respectively, as follows.

First fixed-point P for building A is as follows:

$$\xi_P^2 = \frac{1+\mu}{2\mu}. \tag{A.16}$$

Second fixed-pointQ for building B is as follows:

$$\xi_Q^2 = \frac{1+\mu}{2\mu^2}. \tag{A.17}$$

Thus, the optimum damping ratios for both buildings can be obtained, and the peak transmissibilities at P and Q can be determined. For building A, first, equation (A.13) is substituted into equation (A.2), which yields the following expression:

$$\left(\frac{X_A}{Y}\right)^2 = \frac{\left(1-\mu^2\xi^2\right)^2\xi^4 + 4\mu^2(1+\mu)^2h_J^2\xi^6}{\left(1-\xi^2\right)^2\left(1-\mu^2\xi^2\right)^2 + 4(1+\mu)^2h_J^2\xi^2\left(1-\mu\xi^2\right)^2}. \tag{A.18}$$

Introducing a new parameter $\lambda = \xi^2$ in equation (A.18) results in the following expression:

$$\left(\frac{X_A}{Y}\right)^2 = \frac{\mu^4\lambda^4 + \left\{4\mu^2(1+\mu)^2h_J^2 - 2\mu^2\right\}\lambda^3 + \lambda^2}{\mu^4\lambda^4 + 2\mu^2\left\{2(1+\mu)^2h_J^2 - \left(1+\mu^2\right)\right\}\lambda^3 + \left\{\mu^4+4\mu^2+1-8\mu(1+\mu)^2h_J^2\right\}\lambda^2 + 2\left\{2(1+\mu)^2h_J^2 - (1+\mu)^2\right\}\lambda + 1}. \tag{A.19}$$

Equation (A.19) is differentiated with respect to λ to obtain the peak at P. The numerator of the differentiated equation is extracted, as follows:

$$\mu^8\lambda^5+\left\{8\mu^5(1+\mu)^2h_J^2-\mu^8-4\mu^6\right\}\lambda^4+\left\{16\mu^3(1+\mu)^4h_J^4-2\mu^3(1+\mu)^2\left(\mu^3+7\mu+4\right)h_J^2+4\mu^6+6\mu^4\right\}\lambda^3 \\ +\left\{-16\mu^2(1+\mu)^4h_J^4+8\mu^2(1+\mu)^2\left(2+\mu^2\right)\right\}\lambda^2+\left\{4\mu^2+1-2(1+\mu)^2\left(1+3\mu^2\right)\right\}\lambda-1=0. \tag{A.20}$$

Substituting

$$\xi_P^2=\frac{1+\mu}{2\mu}=\lambda \tag{A.21}$$

in equation (A.20) results in the following expression:

$$\mu^4(1+\mu)^5+2\mu^2(1+\mu)^4\left\{8(1+\mu)^2h_J^2-\mu^3-4\mu\right\} \\ +4\mu(1+\mu)^3\left\{16(1+\mu)^4h_J^4-2(1+\mu)^2\left(\mu^3+7\mu+4\right)h_J^2+4\mu^3+6\mu\right\} \\ +8\mu(1+\mu)^2\left\{-16(1+\mu)^4h_J^4+8(1+\mu)^2\left(2+\mu^2\right)\right\} \\ +16(1+\mu)\left\{4\mu^2+1-2(1+\mu)^2\left(1+3\mu^2\right)\right\}-32\mu=0. \tag{A.22}$$

This equation can be written in the polynomial form of h_J, as follows:

$$-64\mu(1+\mu)^6(1-\mu)h_J^4+8(1+\mu)^3\left(-\mu^6+6\mu^4-4\mu^3-9\mu^2+12\mu-4\right)h_J^2 \\ -\mu^9-3\mu^8+6\mu^7+18\mu^6-21\mu^5-39\mu^4+48\mu^3+24\mu^2-48\mu+16=0. \tag{A.23}$$

Equation (A.23) satisfies the optimum damping ratio for the second fixed-point$Q$, as introduced in [7]. Alternatively, the second fixed-point$Q$ is changed to the first fixed-point P via coordinate conversion. Equation (A.23) can be solved for the factors not indicated in [7], as follows:

$$-64\mu(1+\mu)^6(1-\mu)h_J^4-8(1+\mu)^3(1-\mu)^4(\mu+2)^2h_J^2+(1-\mu)^5(\mu+2)^4=0. \tag{A.24}$$

For building B, the optimum damping ratio for achieving the peak at Q in the transmissibility equation (A.3) satisfies the following condition:

$$\mu^6\lambda^5+\left\{8\mu^5(1+\mu)^2h_J^2-\mu^4\left(4\mu^2+1\right)\right\}\lambda^4 \\ +\left\{16\mu^3(1+\mu)^4h_J^4-2\mu^2(1+\mu)^2\left(4\mu+1^3+7\mu^2\right)h_J^2+2\mu^4\left(2+3\mu^2\right)\right\}\lambda^3 \\ +\left\{-16\mu^2(1+\mu)^4h_J^4+8\mu^2(1+\mu)^2\left(1+2\mu^2\right)h_J^2-2\mu^4\left(3+2\mu^2\right)\right\}\lambda^2 \\ +\left\{\mu^4\left(4+\mu^2\right)-2\mu^2(1+\mu)^2\left(3+\mu^2\right)\right\}\lambda-\mu^4=0. \tag{A.25}$$

This pairs with equation (A.20).
Substituting

$$\xi_Q^2 = \frac{1+\mu}{2\mu^2} = \lambda, \tag{A.26}$$

in equation (A.25) yields the following expression:

$$\begin{aligned}
&(1+\mu)^5 + 2(1+\mu)^4\left\{8\mu(1+\mu)^2 h_J^2 - \left(1+4\mu^2\right)\right\} \\
&\quad + 4(1+\mu)^3\left\{(16\mu 1+\mu)^4 h_J^4 - 2(1+\mu)^2\left(4\mu^3+7\mu^2+1\right)h_J^2 + 2\mu^2\left(2+3\mu^2\right)\right\} \\
&\quad + 8\mu^2(1+\mu)^2 - \left\{16(1+\mu)^4 h_J^4 + 8(1+\mu)^2\left(1+2\mu^2\right)\right\} \\
&\quad + 16\mu^4(1+\mu)\left\{\mu^2\left(4+\mu^2\right) - 2(1+\mu)^2\left(3+\mu^2\right)\right\}.
\end{aligned} \tag{A.27}$$

This equation can be written in the polynomial form of h_J, as follows:

$$64\mu(1+\mu)^6(1-\mu)h_J^4 - 8(1+\mu)^3(1-\mu)^4(1+2\mu)^2 h_J^2 - (1-\mu)^5(1+2\mu)^4 = 0. \tag{A.28}$$

This equation satisfies the optimum damping ratio for the first fixed-point$P$, as introduced in [7]. Similarly, the first fixed-point$P$ is changed to the second fixed-point$Q$ via coordinate conversion.

Equation (A.24) can be solved with respect to h_J^2 to obtain the optimum $h_{P,J,\mathrm{opt}}$ at P for building A, as follows:

$$h_{P,J,\mathrm{opt}} = -\frac{|1-\mu|(2+\mu)}{2(1+\mu)\sqrt{2(1+\mu)}}. \tag{A.29}$$

Similarly, equation (A.28) can be solved to obtain the optimum $h_{Q,J,\mathrm{opt}}$ at the fixed-point$Q$ for building B, as follows:

$$h_{Q,J,\mathrm{opt}} = -\frac{|1-\mu|(1+2\mu)}{2(1+\mu)\sqrt{2\mu(1+\mu)}}. \tag{A.30}$$

B. Validation Data When El Centro Wave Is Input to 20-DOF Models

The numerical analysis results are indicated as the validation studies when the El Centro wave is input to the 20-DOF models. These results respond to Figures 11–14 with the used models shown in Tables 1–7. Table 11 indicates the peak absolute accelerations, and Table 12 indicates the peak displacements relative to the base. The used gravity acceleration is 9.80665 m/s^2 as the standard value in Japan.

Data Availability

The data that support the findings of this study are available from the corresponding author upon reasonable request.

Conflicts of Interest

The authors declare that they have no conflicts of interest.

Acknowledgments

This study was supported by JSPS KAKENHI (Grant no. 23K04344). The authors appreciate the financial support.

References

[1] Y. Ikeda, "Fundamental equation based on pole allocation for interstory seismic isolation of buildings," *Structural Control and Health Monitoring*, vol. 28, no. 3, p. e2687, 2021.

[2] Y. Matsumoto and Y. Ikeda, "Unified understanding of base seismic isolation, interstory seismic isolation and tuned mass damper for buildings," *Journal of Structural Engineering B*, vol. 68, pp. 367–375, 2022.

[3] Y. Ikeda and Y. Matsumoto, "Unified description of passive vibration control for buildings based on pole allocation applied to three-degree-of-freedom model," *Structural Control and Health Monitoring*, vol. 29, no. 9, p. e2995, 2022.

[4] Y. Matsumoto and Y. Ikeda, "Governing equation based on pole allocation for multi-lumped-mass stick-shape shear building model," *Journal of Structural Engineering B*, vol. 69, pp. 1–9, 2023.

[5] J. E. Luco and F. C. P. De Barros, "Optimal damping between two adjacent elastic structures," *Earthquake Engineering and Structural Dynamics*, vol. 27, no. 7, pp. 649–659, 1998.

[6] E. Tubaldi, "Dynamic behavior of adjacent buildings connected by linear viscous/viscoelastic dampers: dynamic behavior of adjacent buildings connected with dampers," *Structural Control and Health Monitoring*, vol. 22, no. 8, pp. 1086–1102, 2015.

[7] K. Iwanami, K. Suzuki, and K. Seto, "Studies of the vibration control method of parallel structures (The method by the theory of P, T, Q)," *Transactions of The Japan Society of Mechanical Engineers Series C*, vol. 52, no. 484, pp. 3063–3072, 1986.

[8] J. P. Den Hartog, *Mechanical Vibrations*, McGraw-Hill, New York, NY, USA, 4th edition, 1956.

[9] A. V. Bhaskararao and R. S. Jangid, "Optimum viscous damper for connecting adjacent SDOF structures for

harmonic and stationary white-noise random excitations," *Earthquake Engineering and Structural Dynamics*, vol. 36, no. 4, pp. 563–571, 2007.

[10] K. Iwanami, K. Suzuki, and K. Seto, "Vibration control method of parallel structures connected to each other with damper and spring," *Transactions of The Japan Society of Mechanical Engineers Series C*, vol. 59, no. 566, pp. 2975–2980, 1993.

[11] M. Kageyama, Y. Yasui, and K. Seto, "The principal solutions of connected spring and damper for optimum vibration control under several criteria," *Journal of Structural and Construction Engineering (Transactions of AIJ)*, vol. 529, pp. 97–104, 2000.

[12] A. Richardson, K. K. Walsh, and M. M. Abdullah, "Closed-form equations for coupling linear structures using stiffness and damping elements," *Structural Control and Health Monitoring*, vol. 20, no. 3, pp. 259–281, 2013.

[13] A. Richardson, K. K. Walsh, and M. M. Abdullah, "Closed-form design equations for controlling vibrations in connected structures," *Journal of Earthquake Engineering*, vol. 17, no. 5, pp. 699–719, 2013.

[14] T. Aida, T. Aso, K. Takeshita, T. Takiuchi, and T. Fujii, "Improvement of the structure damping performance by interconnection," *Journal of Sound and Vibration*, vol. 242, no. 2, pp. 333–353, 2001.

[15] M. Basili, M. De Angelis, and D. Pietrosanti, "Defective two adjacent single degree of freedom systems linked by spring-dashpot-inerter for vibration control," *Engineering Structures*, vol. 188, pp. 480–492, 2019.

[16] E. Mitsuda, M. Ohbuchi, M. Tsuji, and I. Takewaki, "Fundamental properties on eigenvibration and damping in connected building structures," *Journal of Structural and Construction Engineering (Transactions of AIJ)*, vol. 79, no. 696, pp. 227–236, 2014.

[17] H. P. Zhu and H. Iemura, "A study of response control on the passive coupling element between two parallel structures," *Structural Engineering and Mechanics*, vol. 9, no. 4, pp. 383–396, 2000.

[18] V. Gattulli, F. Potenza, and M. Lepidi, "Damping performance of two simple oscillators coupled by a visco-elastic connection," *Journal of Sound and Vibration*, vol. 332, no. 26, pp. 6934–6948, 2013.

[19] Y. Guijun, R. Iwasaki, and T. Takada, "Partioning of mass and frequency ratio space based on invariant point theory of connected buildings and derivation of optimum parameters," *Journal of Structural and Construction Engineering (Transactions of AIJ)*, vol. 72, pp. 71–76, 2007.

[20] T. Ito, M. Tsuji, S. Yoshitomi, and I. Takewaki, "Inverse problem approach to stiffness-damping design of outer-frame type seismic retrofitting," *Journal of Structural and Construction Engineering (Transactions of AIJ)*, vol. 73, no. 627, pp. 725–732, 2008.

[21] A. Reggio, L. Restuccia, and G. A. Ferro, "Feasibility and effectiveness of exoskeleton structures for seismic protection," *Procedia Structural Integrity*, vol. 9, pp. 303–310, 2018.

[22] A. Reggio, L. Restuccia, L. Martelli, and G. A. Ferro, "Seismic performance of exoskeleton structures," *Engineering Structures*, vol. 198, Article ID 109459, 2019.

[23] G. Pipitone, G. Barone, and A. Palmeri, "Optimal design of double-skin façades as vibration absorbers: optimal design of double-skin façades as vibration absorbers," *Structural Control and Health Monitoring*, vol. 25, no. 2, Article ID e2086, 2018.

[24] G. Pipitone, G. Barone, and A. Palmeri, "Stochastic design of double-skin façades as seismic vibration absorbers," *Advances in Engineering Software*, vol. 142, Article ID 102749, 2020.

[25] T. S. Fu, "Double skin façades as mass dampers," in *Proceedings of the American Control Conference (ACC)*, pp. 4742–4746, Atlanta, GA, USA, June, 2013.

[26] K. Sun Moon, "Structural design of double skin facades as damping devices for tall buildings," *Procedia Engineering*, vol. 14, pp. 1351–1358, 2011.

[27] M. Murase and I. Takewaki, "Optimum specifications of inertial mass damper used for building connection system," *Journal of Structural and Construction Engineering (Transactions of AIJ)*, vol. 86, no. 784, pp. 912–923, 2021.

[28] V. Gattulli, F. Potenza, and B. F. Spencer, "Design criteria for dissipative devices in coupled oscillators under seismic excitation," *Structural Control and Health Monitoring*, vol. 25, no. 7, p. e2167, 2018.

[29] Y. L. Xu, Q. He, and J. M. Ko, "Dynamic response of damper-connected adjacent buildings under earthquake excitation," *Engineering Structures*, vol. 21, no. 2, pp. 135–148, 1999.

[30] W. S. Zhang and Y. L. Xu, "Dynamic characteristics and seismic response of adjacent buildings linked by discrete damper," *Earthquake Engineering and Structural Dynamics*, vol. 27, no. 7, pp. 1163–1185, 1999.

[31] H. P. Zhu, D. D. Ge, and X. Huang, "Optimum connecting dampers to reduce the seismic responses of parallel structures," *Journal of Sound and Vibration*, vol. 330, no. 9, pp. 1931–1949, 2011.

[32] Y. Ikeda, "Active and semi-active vibration control of buildings in Japan –Practical Applications and verification," *Structural Control and Health Monitoring*, vol. 16, no. 7–8, pp. 703–723, 2009.

[33] Y. Fujino, D. M. Siringoringo, Y. Ikeda, T. Nagayama, and T. Mizutani, "Research and implementations of structural monitoring for bridges and buildings in Japan," *Engineering*, vol. 5, no. 6, pp. 1093–1119, 2019.

[34] R. W. Clough and J. Penzien, *Dynamics of Structures*, McGraw-Hill Book Company, Singapore, 1982.

[35] S. D. Bharti, S. M. Dumne, and M. K. Shrimali, "Seismic response analysis of adjacent buildings connected with MR dampers," *Engineering Structures*, vol. 32, no. 8, pp. 2122–2133, 2010.